Scattering of radio frequency waves by cylindrical density filaments in tokamak plasmas

Citation: Ram, Abhay K., and Hizanidis, Kyriakos. "Scattering of Radio Frequency Waves by Cylindrical Density Filaments in Tokamak Plasmas." Physics of Plasmas 23, 2 (February 2016): 022504 © 2016 AIP Publishing

As Published: http://dx.doi.org/10.1063/1.4941588

Publisher: American Institute of Physics (AIP)

Persistent URL: http://hdl.handle.net/1721.1/111209

Version: Author's final manuscript: final author's manuscript post peer review, without publisher's formatting or copy editing

PSFC/JA-15-60

Scattering of radio frequency waves by cylindrical density filaments in tokamak plasmas

A. K. Ram and K. Hizanidis[a]

[a]National Technical University of Athens
School of Electrical and Computer Engineering
Association EURATOM-Hellenic Republic, GR-15773, Greece

Plasma Science and Fusion Center,
Massachusetts Institute of Technology
Cambridge, MA 02139 U.S.A.

December 2015

This work was supported by the U.S. Department of Energy grants DE-FG02-91ER-54109, DE-FG02-99ER-54525-NSTX, and DE-FC02-01ER54648, and by the Hellenic National Programme on Controlled Thermonuclear Fusion associated with the EUROfusion Consortium.

Submitted for publication to *Physics of Plasmas* (2015)

Scattering of radio frequency waves by cylindrical density filaments in tokamak plasmas

Abhay K. Ram[1] and Kyriakos Hizanidis[2]

[1]*Plasma Science and Fusion Center,*

Massachusetts Institute of Technology, Cambridge, MA 02139.

[2]*National Technical University of Athens,*

School of Electrical and Computer Engineering,

Association EURATOM-Hellenic Republic, GR-15773, Greece

Abstract

In tokamak fusion plasmas, coherent fluctuations in the form of blobs or filaments are routinely observed in the scrape-off layer. Radio frequency (RF) electromagnetic waves, excited by antenna structures placed near the wall of a tokamak, have to propagate through the scrape-off layer before reaching the core of the plasma. While the effect of fluctuations on the properties of RF waves has not been quantified experimentally, it is of interest to carry out a theoretical study to determine if fluctuations can affect the propagation characteristics of RF waves. Usually, the difference between the plasma density inside the filament and the background plasma density is sizable; the ratio of the density difference to the background density being of order one. Generally, this precludes the use of geometrical optics in determining the effect of fluctuations since the relevant ratio has to be much less than one; typically, of the order of 10% or less. In this paper, a full-wave, analytical model is developed for the scattering of a RF plane wave by a cylindrical plasma filament. It is assumed that the plasma inside and outside the filament is cold and uniform, and that the major axis of the filament is aligned along the toroidal magnetic field. The ratio of the density inside the filament to the density of the background plasma is not restricted. The theoretical framework applies to the scattering of any cold plasma wave. In order to satisfy the boundary conditions at the interface between the filament and the background plasma, the electromagnetic fields inside and outside the filament need to have the same $k_{\|}$, the wave vector parallel to the ambient magnetic field, as the incident plane wave. Consequently, in contrast to the scattering of a RF wave by a spherical blob [A. K. Ram, K. Hizanidis, and Y. Kominis, *Phys. Plasmas* **20**, 056110-1–056110-10 (2013)], the scattering by a field-aligned filament does not broaden the $k_{\|}$ spectrum. However, the filament induces side-scattering leading to surface waves, and can also couple some power to the cold plasma wave different from the incident wave. The changes induced by a filament in the propagation of electron cyclotron waves and lower hybrid waves are illustrated by numerical results displaying the properties of the Poynting vector. The Poynting flux in the wake of the filament, and directed towards the core of the plasma, develops a spatial structure due to diffraction and shadowing. Thus, the fluctuations affect the uniformity of power flow into the plasma.

PACS numbers: 52.20.Dq, 52.65.Cc

I. INTRODUCTION

The scrape-off layer in a tokamak fusion plasma is replete with incoherent and coherent fluctuations – the latter being intermittent and in the form of blobs and filaments [1–9]. The edge plasma plays an important role in the transport of energy and particles to the divertor region and the plasma facing components, as well as in the fusion performance of the core plasma. In this paper, the role of the intermittent, coherent fluctuations on the coupling and propagation of radio frequency (RF) waves is examined.

Radio frequency waves, commonly used for heating the plasma and for generating non-inductive plasma current, are excited by an external antenna structure at the edge of a fusion device. The RF waves have to propagate through the turbulent scrape-off layer on their way toward the core of the plasma. While the effect of blobs and filaments on the RF waves has not been quantified experimentally, a theoretical study is undertaken to determine if the propagation of RF waves is modified by coherent fluctuations. The physical reason that such a study is relevant is quite straightforward. Since the plasma permittivity inside the filaments is different compared to the background plasma, the characteristic properties of the incident RF waves can change during their transit through the fluctuations. This is clearly the case in the conventional propagation of electromagnetic waves through different dielectric media [10]. It is common to study these changes using the geometric optics approximation (see [11] and references therein), wherein, rays, representing plane waves, are refracted due to changes in the plasma permittivity. However, the domain of validity of this approximation is quite limited; it requires that $\delta n \equiv |n_f - n_b|/n_b \ll 1$ (n_f is the density of electrons inside the fluctuation and n_b is the background density). However, from experimental observations, typically, $\delta n \in (0.05, 1)$ in the scrape-off layer [5, 6]. Consequently, a description of the scattering process requires a more general approach that is not limited by the bounds of the geometric optics approximation.

A full-wave theoretical model, using Maxwell's equations, is developed in this paper so as to describe the scattering of a RF plane wave by density filaments. The model is based on the conventional Mie theory for scattering of vacuum electromagnetic waves by spherical dielectrics [12, 13]. The model advanced in this paper is appropriate for magnetized plasmas for which the permittivity is given by a tensor, rather than a scalar. It follows previous studies on the scattering of RF waves by spherical blobs [14, 15], but pertains to scattering

off a cylindrical filament with its axis aligned along the magnetic field line.

In order to understand the effect of the filament on RF fields, and to remain consistent with the approximations described below, it is appropriate to study the wave fields in close proximity of the filament. Observations point to filaments having a correlation length of meters along the magnetic field line, and ranging from 0.1 cm to 10 cm perpendicular to the magnetic field [2, 6]. The RF beam size, limited by the toroidal extent of the antenna structures, is small compared to the size of the filament along the magnetic field line. It is also small compared to the toroidal circumference of the tokamak. Thus, the toroidal plasma is assumed to have a large aspect ratio; in fact, it is approximated by an infinitely extended slab in the direction of the magnetic field. The filament is assumed to be cylindrical and of infinite axial extent along the magnetic field. The latter requirement is essentially needed to ignore the effects due to the ends of a filament of finite axial length. There are two distinct methods that can be followed for a finite size filament. The first method is to use the tangential electric and magnetic fields of the waves on the surface of the filament to construct the far-field solution, by integrating over the finite surface of the cylinder without the end caps [16]. This technique is followed in studies on the scattering of electromagnetic waves by a dielectric cylinder with scalar permittivity, [16]. It is limited to finding the far-fields and not the fields in the vicinity of the filament. The far-field will be affected by the inhomogeneities in the background plasma. The second method is more general and includes the effect of the end caps by imposing the appropriate electromagnetic boundary conditions in the axial direction. However, both of these formulations are well beyond the scope of this paper.

The affect of the filament on a RF plane wave is modeled within the vicinity of the filament. Therefore, it is assumed that the background plasma around the filament has uniform density. Thermal effects in the scrape-off layer are ignored, and the permittivity is that of a cold plasma. The plasma inside the filament is assumed to be cold and uniform. However, δn is allowed to be completely arbitrary and not limited to small density fluctuations. The theoretical framework applies to plasma waves of any frequency, including ion cyclotron, lower hybrid, and electron cyclotron waves.

Beyond their respective domain of validity, there are three primary differences between the full-wave theory and the geometric optics approximation. First, whereas geometric optics is used for describing refractive changes in the ray propagation, the full-wave model also

includes effects due to reflection, diffraction, and shadowing. Second, in geometric optics, the character of the wave does not change as the RF ray propagates through fluctuations. For example, an incident ordinary wave in the electron cyclotron range of frequencies will remain an ordinary wave during its encounter with fluctuations. In the full-wave model, the fluctuations can couple power to other plasma waves. Thus, for the example considered, the ordinary wave couples power to the extraordinary wave. This is not nonlinear parametric coupling; it is linear coupling facilitated by the fluctuations. Third, due to diffraction of waves by the filament, the scattered waves propagate in all radial directions relative to the magnetic field line. Consequently, fluctuations can scatter some of the incident wave power to surface waves which do not propagate into the core plasma. And, for an incident plane wave, the Poynting vector of the scattered waves, directed towards to the core of the plasma, is spatially inhomogeneous. These effects cannot be described within the geometric optics approximation.

There is one important and interesting difference between scattering by a cylindrical filament and scattering by a spherical blob [14, 15]. The kinematic property of the electromagnetic boundary conditions [17], which have to be necessarily satisfied at the interface between the filament and the background plasma, requires that $k_{\|}$ be preserved during the scattering process. In other words, the electromagnetic fields inside and outside the filament have the same $k_{\|}$ as the incoming plane wave. For scattering off a spherical blob this is not the case – $k_{\|}$ is not preserved across the interface and, consequently, the scattered wave has a broad spectrum in $k_{\|}$ [14, 15]. For the filament, the kinematic boundary conditions decouple the azimuthal modes so that the scattering is essentially two dimensional – a consequence of the axis of the cylinder being aligned along the direction of the magnetic field. For the spherical blob, for each azimuthal mode, the polar modes are coupled and the scattering is three dimensional.

From experimental observations, the speed of propagation of the filaments and blobs is of the order of 5×10^3 m s^{-1} [2, 3]. This is orders of magnitude slower than the group velocity, typically near the speed of light, of the usual RF waves used in experiments. The frequency of temporal variation of the fluctuations is less than 1 MHz, which is at least an order of magnitude slower than the frequency of the RF waves. Consequently, in the model, the filament is treated as stationary, with the density inside the filament being uniform in time.

The approach taken to develop the scattering model in this paper can be broadly stated as follows. The formalism, guided by the filament, is carried out in the cylindrical coordinate system. The Faraday-Ampere equation for the electromagnetic fields inside and outside the filament uses the anisotropic, cold plasma permittivity. Its form is that of the vector Helmholtz equation which can be solved by classical techniques using the vector cylinder functions [19]. The electromagnetic fields of the incident plane wave, the scattered waves, and the waves inside the filament are all expressed in terms of the vector cylinder functions. The boundary conditions at the interface between the filament and the background plasma couple the amplitudes of these waves. For each azimuthal mode number, a set of four, coupled, algebraic equations are obtained. The polarizations of the waves and their propagation characteristics are all included in these coupled equations. The four-equation set can be solved for the amplitudes of the fields inside and outside the filament in terms of the amplitude of the incident wave. The total fields are obtained by summing up the contributions from all the azimuthal components.

Section II summarizes the assumptions, the approximations, and the geometry that are used in the scattering. The Faraday-Ampere equation for the wave fields, along with the cold plasma permittivity are set up in Section III. The expression for a plane wave in terms of the vector cylinder functions is derived in Section IV, which is followed by a description of a plane wave in a plasma in Section V. The dispersion characteristics of a plane wave, the identification of two wave modes that propagate in a cold plasma, and the corresponding polarizations and wave electric fields are also set up in Section V. The boundary conditions that need to be satisfied at the interface of the filament and the background plasma are stated in Section VI. The kinematic property of the boundary conditions requires that all waves have the same $k_{\parallel}$ as the incoming plane wave. The electric fields of the waves inside the filament and of the scattered waves outside the filament are obtained in Sections VII and VIII, respectively. The algebraic equations which, self consistently, couple the incident plane wave, the waves inside the filament, and the scattered waves outside the filament are obtained from the dynamic properties of the boundary conditions in Section IX. At this stage the theoretical formulation of the scattering of RF waves by a cylindrical filament is complete. In Section X, the theory is applied to the scattering of waves in the electron cyclotron and lower hybrid range of frequencies for parameters corresponding to a high density and high magnetic field plasma. These parameters could be representative of an

ITER-type edge plasma. However, the main purpose of this section is to illustrate the physics of scattering of RF waves by a filament with a density that is different from the density of the background plasma.

II. DESCRIPTION OF THE GEOMETRY AND THE PLASMA

We assume that a cylindrical filament, with a circular cross-section, has its axis aligned along the ambient magnetic field line (Fig. 1). The axial extent of the filament is taken to be infinite; this is a valid approximation if the RF beam width along the axial direction is smaller than the length of the filament. Consequently, any effects due to the ends of a finite-size filament are neglected. The density of the background plasma in which the filament exists, and the density inside the filament are assumed to be spatially homogeneous with the entire plasma being cold. There is no limitation on the ratio of the two densities.

The relationship between the cylindrical coordinate system ($\widehat{\boldsymbol{\rho}},\ \widehat{\boldsymbol{\phi}},\ \widehat{\mathbf{z}}$), used as a basis in the theory, and the Cartesian coordinate system ($\widehat{\mathbf{x}},\ \widehat{\mathbf{y}},\ \widehat{\mathbf{z}}$) can be expressed in the form taken by the position vector $\mathbf{r}$ (Appendix A),

$$\mathbf{r} \ = \ x\,\widehat{\mathbf{x}} \ + \ y\,\widehat{\mathbf{y}} \ + \ z\,\widehat{\mathbf{z}} \ = \ \rho\,\widehat{\boldsymbol{\rho}} \ + \ z\,\widehat{\mathbf{z}}, \tag{1}$$

where $\rho = \sqrt{x^2 + y^2}$, and z is along the axial direction. The origin of the coordinate system is the center of the cylindrical filament. The ambient magnetic field in which the plasma and the filament are immersed is taken to be uniform and along the z-direction.

III. PROPAGATION OF ELECTROMAGNETIC WAVES IN A PLASMA

For a cold fluid plasma, described by a linearized set of continuity and momentum equations for electrons and ions, Faraday's and Ampere's equations in Maxwell's system of equations can be combined [18] to yield the following equation for the spatial variation of the electric field,

$$\nabla \times \nabla \times \mathbf{E}\,(\mathbf{r}) - \frac{\omega^2}{c^2}\ \overleftrightarrow{\mathbf{K}}\,(\mathbf{r})\,.\,\mathbf{E}\,(\mathbf{r}) \ = \ 0, \tag{2}$$

where ω is the angular frequency of the perturbed electromagnetic fields and densities, c is the speed of light, and $\overleftrightarrow{\mathbf{K}}\,(\mathbf{r})$ is plasma permittivity tensor. We have assumed that the plasma equilibrium is time independent, while the linearized perturbed electromagnetic

fields, and electron and ion densities, have a time dependence of the form $\mathrm{e}^{-i\omega t}$, where t is the time. In the cylindrical coordinate system where the ambient magnetic field $\mathbf{B}_0 = B_0\widehat{\mathbf{z}}$ is aligned along the z-axis, $\overleftrightarrow{\mathbf{K}}(\mathbf{r})$ has the form [18]

$$\overleftrightarrow{\mathbf{K}} = \begin{pmatrix} K_\rho & -iK_\phi & 0 \\ iK_\phi & K_\rho & 0 \\ 0 & 0 & K_z \end{pmatrix}, \tag{3}$$

where

$$\begin{aligned} K_\rho &= 1 - \frac{\omega_{pe}^2}{\omega^2 - \omega_{ce}^2} - \sum_i \frac{\omega_{pi}^2}{\omega^2 - \omega_{ci}^2}, \\ K_\phi &= -\frac{\omega_{ce}}{\omega}\frac{\omega_{pe}^2}{\omega^2 - \omega_{ce}^2} + \sum_i \frac{\omega_{ci}}{\omega}\frac{\omega_{pi}^2}{\omega^2 - \omega_{ci}^2}, \\ K_z &= 1 - \frac{\omega_{pe}^2}{\omega^2} - \sum_i \frac{\omega_{pi}^2}{\omega^2}, \end{aligned} \tag{4}$$

ω_{pe} (ω_{pi}) and ω_{ce} (ω_{ci}) are the angular electron (ion) plasma frequency and cyclotron frequency, respectively, and the index i represents all the ion species in the plasma. The plasma and cyclotron frequencies can, in general, be functions of space. The permittivity tensor of the background plasma and of the filament are expressed in terms of their respective ion compositions and constant, but different, densities. Subsequently, the elements of $\overleftrightarrow{\mathbf{K}}$ are constants in each region.

The electromagnetic wave equation (2) has the form of a vector Helmholtz equation. It is solved in the cylindrical coordinate system using the vector cylinder functions discussed in Appendix B.

IV. REPRESENTATION OF A PLANE WAVE IN VECTOR CYLINDER FUNCTIONS

In cylindrical coordinates, the spatial variation of a plane wave is [19],

$$e^{i\mathbf{k}.\mathbf{r}} = e^{ik_\rho\rho\cos(\phi-\phi_k) + ik_z z} = \sum_{m=-\infty}^{\infty} i^m \, \mathrm{J}_m\left(k_\rho\rho\right) e^{im(\phi-\phi_k)} \, e^{ik_z z}, \tag{5}$$

where J_m is the Bessel function of the first kind of order m. In this representation, ϕ and ϕ_k are the azimuthal angles between the x-axis and $\mathbf{r}$ and $\mathbf{k}$, respectively, and $k_\rho = \sqrt{k_x^2 + k_y^2}$. The Cartesian coordinate components of $\mathbf{k}$ are k_x, k_y, and k_z. From (69) in Appendix B, it follows that,

$$\begin{pmatrix} \widehat{\boldsymbol{\rho}} \\ \widehat{\boldsymbol{\phi}} \\ \widehat{\mathbf{z}} \end{pmatrix} e^{i\mathbf{k}.\mathbf{r}} \;=\; \sum_{m=-\infty}^{\infty} i^m \, e^{-im\phi_k} \;\left(\mathbf{al}_{1m} \;+\; \mathbf{bm}_{1m} \;+\; \mathbf{cn}_{1m} \right). \tag{6}$$

The right-hand side is a sum of three dyadics, and the column vectors $\mathbf{a}$, $\mathbf{b}$, and $\mathbf{c}$ are given by

$$\mathbf{a} \;=\; \frac{i}{k^2} \begin{pmatrix} -k_\rho \cos\left(\phi - \phi_k\right) \\ k_\rho \sin\left(\phi - \phi_k\right) \\ -k_z \end{pmatrix}, \mathbf{b} \;=\; \frac{i}{k_\rho} \begin{pmatrix} \sin\left(\phi - \phi_k\right) \\ \cos\left(\phi - \phi_k\right) \\ 0 \end{pmatrix}, \mathbf{c} \;=\; \frac{1}{k k_\rho} \begin{pmatrix} -k_z \cos\left(\phi - \phi_k\right) \\ k_z \sin\left(\phi - \phi_k\right) \\ k_\rho \end{pmatrix}. \tag{7}$$

The vector cylinder functions $\mathbf{l}_{1m}$, $\mathbf{m}_{1m}$, and $\mathbf{n}_{1m}$ are the same as $\mathbf{l}_m$, $\mathbf{m}_m$, and $\mathbf{n}_m$, respectively, given in (69) in Appendix B, except with $\mathcal{Z}_m$ replaced by J_m.

V. FORMULATING THE INCOMING PLANE WAVE

The incoming RF plane wave, propagating in the background plasma and impinging on the filament, is taken to be of the form

$$\mathbf{E}_I\left(\mathbf{r}\right) \;=\; \mathbf{E}_0\left(\mathbf{k}_0, \omega\right) \; e^{i\mathbf{k}_0.\mathbf{r}}, \tag{8}$$

where $\mathbf{E}_0$ is the electric field vector which is independent of space and time, and $\mathbf{k}_0$ is the wave vector of the plane wave. Substituting this form into Eq. (2) yields,

$$\overleftrightarrow{\mathbf{D}}_0\left(\mathbf{k}_0, \omega\right) \;.\; \mathbf{E}_0\left(\mathbf{k}_0, \omega\right) \;=\; 0, \tag{9}$$

where

$$\overleftrightarrow{\mathbf{D}}_0\left(\mathbf{k}_0, \omega\right) \;=\; \frac{c^2}{\omega^2}\left(\mathbf{k}_0\mathbf{k}_0 - k_0^2 \overleftrightarrow{\mathbf{I}}\right) \;+\; \overleftrightarrow{\mathbf{K}}_0. \tag{10}$$

Here $\mathbf{k}_0\mathbf{k}_0$ is a dyadic, $\overleftrightarrow{\mathbf{I}}$ is the unit tensor, and $\overleftrightarrow{\mathbf{K}}_0$ is the plasma permittivity $\overleftrightarrow{\mathbf{K}}$, given by Eq. (3), of the background plasma. For a non-trivial solution of the wave electric field, we require that

$$\det\left(\overleftrightarrow{\mathbf{D}}_0\left(\mathbf{k}_0, \omega\right)\right) \;=\; 0 \tag{11}$$

where det denotes the determinant of the tensor. Using (10) in (11) leads to the following algebraic equation,

$$n_{0\rho}^4 K_{0\rho} \; + \; n_{0\rho}^2 \left[K_{0\phi}^2 - \left(K_{0\rho} + K_{0z} \right) \left(K_{0\rho} - n_{0z}^2 \right) \right] \; + \; K_{0z} \left[\left(K_{0\rho} - n_{0z}^2 \right)^2 - K_{0\phi}^2 \right] \; = \; 0, \quad (12)$$

where the index of refraction $\mathbf{n}_0 = c\mathbf{k}_0/\omega$ has the components $(n_{0\rho}, 0, n_{0z})$ in the cylindrical coordinate system determined by $\mathbf{k}_0$.

A. Dispersion characteristics of the wave

In experiments, the spectrum of the launched waves, along the direction of the magnetic field, is determined by the antenna structure exciting the RF fields. For a given set of plasma parameters, and a prescribed n_z – component of the index of refraction along the magnetic field – the algebraic equation (12) is the dispersion relation for the incident plane wave. Its solution gives the magnitude of the $\widehat{\boldsymbol{\rho}}$-component of the wave vector, or index of refraction. The azimuthal symmetry around the magnetic field line eliminates any dependence on the $\widehat{\boldsymbol{\phi}}$-component of the wave vector. There are two solutions of the bi-quadratic equation,

$$\begin{aligned} n_{0\rho\pm}^2 \; = \; & \frac{1}{2K_{0\rho}} \left(K_{0\rho} + K_{0z} \right) \left(K_{0\rho} - n_{0z}^2 \right) \; - \; \frac{1}{2K_{0\rho}} K_{0\phi}^2 \\ & \pm \; \frac{1}{2K_{0\rho}} \sqrt{\left[\left\{ \left(K_{0\rho} - K_{0z} \right) \left(K_{0\rho} - n_{0z}^2 \right) - K_{0\phi}^2 \right\}^2 \; + \; 4 n_{0z}^2 K_{0\phi}^2 K_{0z} \right]}. \quad (13) \end{aligned}$$

The four values of $n_{0\rho}$ follow trivially from (13). In order to ensure that there are two distinct solutions to $n_{0\rho}^2$, the expression under the radical is assumed to be greater that zero. If this expression is zero then the two solutions to $n_{0\rho}^2$ are degenerate, and if it is negative the two roots are complex conjugate pairs. In RF heating and current drive experiments, the frequency of the launched wave is chosen so as to avoid such a situation in the edge region of the plasma. Otherwise, the wave power coupled into the core of the plasma is significantly reduced.

The roots of the dispersion relation (13) are classified in the following way. For waves propagating across the magnetic field $n_{0z} = 0$, (13) yields,

$$n_{0\rho+}^2 \; = \; \frac{K_{0\rho}^2 - K_{0\phi}^2}{K_{0\rho}}, \quad (14)$$

$$n_{0\rho-}^2 \; = \; K_{0z}. \quad (15)$$

In the electron cyclotron range of frequencies (14) is the extraordinary wave dispersion relation, while (15) is that for the ordinary wave. In the lower hybrid range of frequencies these are referred to as the fast and slow lower hybrid waves, respectively. In the ion cyclotron range of frequencies these are the fast Alfvén wave and slow Alfvén wave, respectively. The two wave modes obtained from (13) will be denoted by $n_{0\rho X}^2$ and $n_{0\rho O}^2$ with the understanding that for $n_{0z} \to 0$, they approach (14) and (15), respectively. The subscripts X and O refer to the extraordinary, or fast, wave and the ordinary, or slow, wave, respectively.

B. Wave polarizations

The electric field $\mathbf{E}_0$ in (8) can be written as,

$$\mathbf{E}_0\left(\mathbf{k}_0,\omega\right) \;=\; \mathcal{E}_0\left(E_{0k\rho}\widehat{\boldsymbol{\rho}}_k \;+\; E_{0k\phi}\widehat{\boldsymbol{\phi}}_k \;+\; E_{0kz}\widehat{\mathbf{z}}\right), \tag{16}$$

where $\mathcal{E}_0$ is the amplitude of the electric field, and $(E_{0k\rho}, E_{0k\phi}, E_{0kz})$ are the components of the polarization vector along $\left(\widehat{\boldsymbol{\rho}}_k, \widehat{\boldsymbol{\phi}}_k, \widehat{\mathbf{z}}\right)$. The polarization of the wave electric field follows from (9).

For numerical implementation of the theoretical model, it is suitable to define the wave polarizations differently for the X and O waves. For the X, or fast, wave, the components of the wave polarization vector are,

$$\begin{aligned} e_{Xk\rho} \;&=\; 1, \\ e_{Xk\phi} \;&=\; -\frac{iK_{0\phi}}{K_{0\rho} - n_{0\rho X}^2 - n_{0z}^2}, \\ e_{Xkz} \;&=\; -\frac{n_{0\rho X} n_{0z}}{K_{0z} - n_{0\rho X}^2}. \end{aligned} \tag{17}$$

For the O, or slow, wave, the components of the wave polarization vector are,

$$\begin{aligned} e_{Ok\rho} \;&=\; -\frac{n_{0\rho 0} n_{0z}\left(K_{0\rho} - n_{0\rho O}^2 - n_{0z}^2\right)}{\left(K_{0\rho} - n_{0z}^2\right)\left(K_{0\rho} - n_{0\rho O}^2 - n_{0z}^2\right) - K_{0\phi}^2} \\ e_{Ok\phi} \;&=\; -\frac{in_{0\rho O} n_{0z} K_{0\phi}}{\left(K_{0\rho} - n_{0z}^2\right)\left(K_{0\rho} - n_{0\rho O}^2 - n_{0z}^2\right) - K_{0\phi}^2} \\ e_{Okz} \;&=\; 1. \end{aligned} \tag{18}$$

The components $(E_{0k\rho}, E_{0k\phi}, E_{0kz})$ in (16) are defined as,

$$\left(E_{0k\rho}, E_{0k\phi}, E_{0kz}\right) \;=\; \frac{1}{\sqrt{\left|e_{k\rho}\right|^2 + \left|e_{k\phi}\right|^2 + \left|e_{kz}\right|^2}}\;\left(e_{k\rho}, e_{k\phi}, e_{kz}\right), \tag{19}$$

with the understanding that the subscripts for the X or O waves are to be included in $(e_{k\rho}, e_{k\phi}, e_{kz})$ as appropriate.

The local characteristics of the plasma wave, launched by an antenna, and propagating toward the filament are now defined. For a prescribed n_{0z}, the wave number perpendicular to the magnetic field $n_{0\rho}$ is given by one of the four roots of (13). The corresponding wave electric field and polarization are obtained, as appropriate, from (19).

C. Electric field of the wave

The propagation characteristics and the electric field polarization of the incoming plane wave have been determined in the $\left(\widehat{\boldsymbol{\rho}}_k, \widehat{\boldsymbol{\phi}}_k, \widehat{\mathbf{z}}\right)$ coordinates. The electric field vector can be expressed in terms of the vector cylinder functions by transforming Eqs. (6) and (7) from the $\left(\widehat{\boldsymbol{\rho}}, \widehat{\boldsymbol{\phi}}, \widehat{\mathbf{z}}\right)$ coordinate system to the $\left(\widehat{\boldsymbol{\rho}}_k, \widehat{\boldsymbol{\phi}}_k, \widehat{\mathbf{z}}\right)$ coordinate system by applying the rotation matrices $\left(\overleftrightarrow{\mathcal{R}}_\rho\right)^{-1}$ and $\overleftrightarrow{\mathcal{R}}_k$ successively (Appendix A). Then,

$$\begin{pmatrix} \widehat{\boldsymbol{\rho}}_k \\ \widehat{\boldsymbol{\phi}}_k \\ \widehat{\mathbf{z}} \end{pmatrix} e^{i\mathbf{k}.\mathbf{r}} = \sum_{m=-\infty}^{\infty} i^m \, e^{-im\phi_k} \, \left(\mathbf{a}_k \mathbf{l}_{1m} + \mathbf{b}_k \mathbf{m}_{1m} + \mathbf{c}_k \mathbf{n}_{1m} \right), \tag{20}$$

where

$$\mathbf{a}_k = \frac{i}{k^2} \begin{pmatrix} -k_\rho \\ 0 \\ -k_z \end{pmatrix}, \mathbf{b}_k = \frac{i}{k_\rho} \begin{pmatrix} 0 \\ 1 \\ 0 \end{pmatrix}, \mathbf{c}_k = \frac{1}{kk_\rho} \begin{pmatrix} -k_z \\ 0 \\ k_\rho \end{pmatrix}, \tag{21}$$

and k is the magnitude of $\mathbf{k}$. The explicit form of the wave electric field is obtained by substituting the expressions in (16), (20), and (21) into (8). The result is,

$$\begin{aligned} \mathbf{E}_I(\mathbf{r}) = \mathcal{E}_0 \sum_{m=-\infty}^{\infty} i^m \Bigg[& \left\{ -iE_{0k\rho} \mathrm{J}'_m(k_{0\rho}\rho) - \frac{m}{\rho k_{0\rho}} E_{0k\phi} \mathrm{J}_m(k_{0\rho}\rho) \right\} \widehat{\boldsymbol{\rho}} + \\ & \left\{ -iE_{0k\phi} \mathrm{J}'_m(k_{0\rho}\rho) + \frac{m}{\rho k_{0\rho}} E_{0k\rho} \mathrm{J}_m(k_{0\rho}\rho) \right\} \widehat{\boldsymbol{\phi}} + \\ & E_{0kz} \mathrm{J}_m(k_{0\rho}\rho) \widehat{\mathbf{z}} \Bigg] \, e^{im(\phi-\phi_k)} \, e^{ik_{0z}z}, \end{aligned} \tag{22}$$

where the prime denotes derivative with respect to the argument.

VI. BOUNDARY CONDITIONS - KINEMATIC PROPERTIES

Even though the electromagnetic wave fields inside the filament and the scattered fields outside the filament have not yet been determined, it is worth considering the implications of the boundary conditions. It turns out that an important simplification arises from the boundary conditions. Assuming that there are no free charges and currents in the interface between the filament and the background plasma, Maxwell's equations impose the following conditions [10],

$$\widehat{\boldsymbol{\rho}}.\left(\mathbf{D}_I+\mathbf{D}_S\right)\Big|_{\rho=a} = \widehat{\boldsymbol{\rho}}.\,\mathbf{D}_F\Big|_{\rho=a}, \tag{23}$$

$$\widehat{\boldsymbol{\rho}}.\left(\mathbf{B}_I+\mathbf{B}_S\right)\Big|_{\rho=a} = \widehat{\boldsymbol{\rho}}.\,\mathbf{B}_F\Big|_{\rho=a}, \tag{24}$$

$$\widehat{\boldsymbol{\rho}}\times\left(\mathbf{E}_I+\mathbf{E}_S\right)\Big|_{\rho=a} = \widehat{\boldsymbol{\rho}}\times\mathbf{E}_F\Big|_{\rho=a}, \tag{25}$$

$$\widehat{\boldsymbol{\rho}}\times\left(\mathbf{B}_I+\mathbf{B}_S\right)\Big|_{\rho=a} = \widehat{\boldsymbol{\rho}}\times\mathbf{B}_F\Big|_{\rho=a}. \tag{26}$$

The subscripts I, S, and F refer to the incident, scattered, and filamentary wave fields, respectively, $\mathbf{D}=\epsilon_0\overleftrightarrow{\mathbf{K}}.\,\mathbf{E}$ is the wave electric displacement field, ϵ_0 is the free-space permeability, and $\mathbf{E}$ and $\mathbf{B}$ are the wave electric and magnetic field, respectively. The four sets of boundary conditions follow from Gauss' law, Gauss' magnetism law, Faraday's law, and Ampere's law, respectively. The left and right sides of Eqs. (23)-(26) are evaluated at the boundary of the filament $\rho=a$.

The boundary conditions must be satisfied for all ϕ and z, and for all times t. Thus, the (ϕ,z,t) variations of all the fields must be the same at $\rho=a$. In particular, as the z and t variation of the incoming electromagnetic wave is $e^{ik_{0z}z-i\omega t}$, the fields inside the filament and the scattered fields must have the same variation with respect to z and t. Consequently, the time variation of all the fields is $e^{-i\omega t}$. And, importantly, the z variation of all the fields is of the form $e^{ik_{0z}z}$ for all z; i.e., the component of the wave vector along the magnetic field is preserved in the scattering process. This is a kinematic property that, for example, in conventional electrodynamics, leads to Snell's law for reflection and refraction of electromagnetic waves at an interface [17]. The dynamic properties [17], such as amplitudes and polarizations of the electromagnetic fields, which follow from boundary conditions will be determined later in this paper.

The simplification that follows from the boundary conditions reduces the scattering pro-

cess to two spatial directions. In contrast, the scattering of RF waves by spherical blobs [14, 15] is three-dimensional, and the component of the wave vector parallel to the magnetic field is not preserved.

VII. ELECTROMAGNETIC FIELDS INSIDE THE FILAMENT

The wave fields inside the filament, a spatially bounded plasma, are obtained from the Faraday-Ampere equation (2) by using the Fourier transform in cylindrical coordinates,

$$\mathbf{E}_F(\mathbf{r}) \;=\; \int d^3k\; \mathbf{E}_F(\mathbf{k})\, e^{i\mathbf{k}.\mathbf{r}} \;=\; \int_0^\infty dk_\rho\; k_\rho \int_0^{2\pi} d\phi_k \int_{-\infty}^{\infty} dk_z\; \mathbf{E}_F(\mathbf{k})\, e^{ik_\rho \rho\cos(\phi-\phi_k)} e^{ik_z z}. \tag{27}$$

Substituting this form in (2) yields

$$\int\; d^3k\; \overleftrightarrow{\mathbf{D}}(\mathbf{k},\omega)\,.\,\mathbf{E}_k(\mathbf{k})\;\; e^{ik_\rho\rho\cos(\phi-\phi_k)} e^{ik_z z} \;=\; 0, \tag{28}$$

where,

$$\overleftrightarrow{\mathbf{D}}(\mathbf{k},\omega) \;=\; \frac{c^2}{\omega^2}\left(\mathbf{kk} - k^2\overleftrightarrow{\mathbf{I}}\right) + \overleftrightarrow{\mathbf{K}}(\omega) \tag{29}$$

is the dielectric tensor corresponding to the plasma parameters inside the filament. Here $\mathbf{kk}$ is a dyadic.

In general, Eq. (28) is satisfied if and only if,

$$\overleftrightarrow{\mathbf{D}}(\mathbf{k},\omega)\,.\,\mathbf{E}_k(\mathbf{k}) \;=\; 0. \tag{30}$$

Since $\mathbf{k} = k_\rho\widehat{\boldsymbol{\rho}}_k + k_z\widehat{\mathbf{z}}$, a non-trivial solution for the $\mathbf{E}_k$ requires that $\det\overleftrightarrow{\mathbf{D}}(\mathbf{k},\omega) = 0$. This requirement, as in Section V, leads to a dispersion relation connecting k_ρ, k_z, and ω. The dispersion relation is the same as in (12) without the index 0; the solutions to the bi-quadratic equation are analogues of (13).

At this stage, in order to simplify the algebra, it is convenient to impose the kinematic property of the boundary conditions, namely that k_z inside the filament is restricted to being the same as for the incoming plane wave. Then, the dispersion relation $\det\overleftrightarrow{\mathbf{D}}(k_\rho, k_z, \omega) = 0$, derived for the plasma parameters inside the filament, is solved for the four branches in k_ρ. However, since the dispersion relation is bi-quadratic in k_ρ, two of the roots are negative of the other two roots. The negative roots, in the cylindrical coordinate system, can be accounted for by a rotation in ϕ_k through π radians. Thus, there are only two independent

wave branches. As a consequence, the Fourier transformed wave field can be written as,

$$\mathbf{E}_F\left(\mathbf{k}\right) \;=\; \sum_{\ell=1}^{2} \mathbf{E}_\ell\left(\mathbf{k}\right) \;\frac{1}{k_\rho}\delta\left(k_\rho - k_{\ell\rho}\right) \;\delta\left(k_z - k_{0z}\right), \tag{31}$$

where the summation is over the two independent wave branches of the dispersion relation, designated by $k_{\ell\rho}$, and δ denotes the Dirac delta function.

Since $\overleftrightarrow{\mathbf{D}}.\,\mathbf{E}_\ell\left(\mathbf{k}\right) = 0$ for $\ell = 1, 2$, $\mathbf{E}_\ell$ can be expressed in terms of an overall electric field amplitude and a polarization vector. Following the discussion on wave polarizations in Section V B,

$$\mathbf{E}_\ell\left(\mathbf{k}\right) \;=\; \mathcal{E}_\ell\left(E_{\ell k\rho}\;\widehat{\boldsymbol{\rho}}_k + E_{\ell k\phi}\;\widehat{\boldsymbol{\phi}}_k + E_{\ell kz}\;\widehat{\mathbf{z}}\right). \tag{32}$$

The components of the polarization vector $\mathbf{E}_\ell^P = E_{\ell k\rho}\widehat{\boldsymbol{\rho}}_k + E_{\ell k\phi}\widehat{\boldsymbol{\phi}}_k + E_{\ell kz}\widehat{\mathbf{z}}$, are as given in Eq. (19), and either (17) or (18). These components depend on $k_{\ell\rho}$, k_{0z}, ω, and the plasma parameters inside the filament. They are not functions of ϕ_k. However, in general, the amplitude $\mathcal{E}_\ell$ can only be a function of ϕ_k; all the other wave and plasma parameters being accounted for in the polarization vector. Any function of the angle ϕ_k has to be periodic in ϕ_k. Thus, $\mathcal{E}_\ell\left(\phi_k\right)$ can be expressed as a complex Fourier series,

$$\mathcal{E}_\ell\left(\phi_k\right) \;=\; \sum_{m'=-\infty}^{\infty} \mathcal{E}_{\ell m'}\; e^{im'\phi_k}, \tag{33}$$

where $\mathcal{E}_{\ell m'}$ is the amplitude of the m'-th Fourier mode.

The wave electric field inside the filament is obtained by substituting (31), (32), and (33) into the right-hand side of (27), and using (20) and (21) for the eikonal $e^{i\mathbf{k}.\mathbf{r}}$. The Dirac delta functions simplify the integrals with respect to k_ρ and k_z. The integral with respect to ϕ_k is,

$$\int_0^{2\pi} d\phi_k\; e^{im'\phi_k} e^{-im\phi_k} \;=\; 2\pi\delta_{m,m'}, \tag{34}$$

where $\delta_{m,m'}$ is the Kronecker delta function.

Finally, the wave electric field inside the filament is,

$$\begin{aligned}\mathbf{E}_F\left(\mathbf{r}\right) \;=\; \sum_{\ell=1}^{2}\sum_{m=-\infty}^{\infty} i^m\;\mathcal{E}_{\ell m}\;\Bigg[&\left\{-iE_{\ell k\rho}\mathrm{J}'_m\left(k_{\ell\rho}\rho\right) - \frac{m}{\rho k_{\ell\rho}}E_{\ell k\phi}\mathrm{J}_m\left(k_{\ell\rho}\rho\right)\right\}\widehat{\boldsymbol{\rho}} + \\ &\left\{-iE_{\ell k\phi}\mathrm{J}'_m\left(k_{\ell\rho}\rho\right) + \frac{m}{\rho k_{\ell\rho}}E_{\ell k\rho}\mathrm{J}_m\left(k_{\ell\rho}\rho\right)\right\}\widehat{\boldsymbol{\phi}} + \\ &E_{\ell kz}\mathrm{J}_m\left(k_{\ell\rho}\rho\right)\widehat{\mathbf{z}}\Bigg]\;e^{im\phi}\;e^{ik_{0z}z},\end{aligned} \tag{35}$$

where, without loss of generality, the factor of 2π from (34) has been absorbed in the coefficient $\mathcal{E}_{\ell m}$.

It is important to note that, regardless of the choice of the incoming wave mode, the wave fields inside the filament are a combination of the two independent cold plasma waves. Thus, if the ordinary wave in the electron cyclotron range of frequencies is incident on the filament, the fields inside the filament are a linear combination of the ordinary and extraordinary waves. The boundary conditions, Eqs. (23)–(26), at the interface between the filament and the background plasma cannot be satisfied without requiring both wave modes to be present inside the filament.

VIII. ELECTRIC FIELDS OF THE SCATTERED WAVES

The construction of the wave fields in the background plasma, due to the scattering by the filament, will take advantage of two points. The first point is that the component of the wave vector along the magnetic field is the same as that of the incident wave – the kinematic property of the boundary conditions. The second point is that the scattered waves are outgoing and propagating away from the filament.

Since the vector cylinder functions form a complete set [19, 20], and are solutions of the vector Helmholtz equation, the electric field of the scattered wave can be written, in general, as a linear sum of the entire set of vector cylinder functions. Thus,

$$\mathbf{E}_S\left(\mathbf{r}\right) \;=\; \sum_{m=-\infty}^{\infty} \left[E_{1m}\mathbf{l}_m\left(\rho,\phi,z;k_\rho,k_{0z}\right) + E_{2m}\mathbf{m}_m\left(\rho,\phi,z;k_\rho,k_{0z}\right) + E_{3m}\mathbf{n}_m\left(\rho,\phi,z;k_\rho,k_{0z}\right)\right], \tag{36}$$

where E_{1m}, E_{2m}, and E_{3m} are coefficients that can, in general, be functions of m and $\mathbf{k}$. In order to ensure an outgoing wave, in the vector cylinder functions (69), $\mathcal{Z}_m\left(k_\rho\rho\right)$ is replaced by the Hankel function of the first kind $\mathrm{H}_m^{(1)}\left(k_\rho\rho\right)$ [21].

The coefficients E_{1m}, E_{2m}, and E_{3m} are determined by substituting (36) into (2). In the resulting equation, the only dependence on ϕ is in the vector cylinder functions, and is of the form $e^{im\phi}$. The orthogonality of these functions forces each term in the summation over m, in the right-hand side of the resulting equation, to be zero. Furthermore, $\mathrm{H}_m^{(1)}\left(k_\rho\rho\right)$ and $\mathrm{H}_m^{(1)\prime}\left(k_\rho\rho\right)$ are independent functions of the argument [21]. (Here the prime denotes a

derivative with respect to the argument.) Subsequently, equating coefficients of $\mathrm{H}_m^{(1)}(k_\rho\rho)$ and $\mathrm{H}_m^{(1)\prime}(k_\rho\rho)$ in each vector component in the equation obtained by substituting (36) into (2), leads to the following set of equations,

$$\begin{aligned} K_{0\rho}E_{1m} + iK_{0\phi}E_{2m} - i\frac{k_{0z}}{k}\left(\frac{c^2k^2}{\omega^2} - K_{0\rho}\right)E_{3m} &= 0, \\ K_{0\phi}E_{1m} - i\left(\frac{c^2k^2}{\omega^2} - K_{0\rho}\right)E_{2m} + i\frac{k_{0z}}{k}K_{0\phi}E_{3m} &= 0, \\ ik_{0z}K_{0z}E_{1m} - \frac{k_\rho^2}{k}\left(\frac{c^2k^2}{\omega^2} - K_{0z}\right)E_{3m} &= 0. \end{aligned} \tag{37}$$

The permittivity tensor elements in (37) are evaluated for the background plasma parameters. The three equations in (37) form a set of homogeneous algebraic equations for E_{1m}, E_{2m}, and E_{3m} and are almost of the form $\overleftrightarrow{\mathbf{D}}_0 . \mathbf{E}_{Sk}(\mathbf{k}) = 0$. Guided by the form of the wave electric field in the filament (35), the following substitutions,

$$\begin{aligned} E_{1m} &= -i\frac{k_\rho}{k^2}E_{k\rho}^S - i\frac{k_z}{k^2}E_{kz}^S, \\ E_{2m} &= \frac{i}{k_\rho}E_{k_\phi}^S, \\ E_{3m} &= -\frac{k_{0z}}{kk_\rho}E_{k\rho}^S + \frac{1}{k}E_{kz}^S, \end{aligned} \tag{38}$$

reduce (37) to,

$$\begin{aligned} \left(K_{0\rho} - n_{0z}^2\right)E_{k\rho}^S - iK_{0\phi}E_{k\phi}^S + n_\rho n_{0z}E_{kz}^S &= 0, \\ iK_{0\phi}E_{k\rho}^S + \left(K_{0\rho} - n^2\right)E_{k\phi}^S &= 0, \\ n_\rho n_{0z}E_{k\rho}^S + \left(K_{0z} - n_\rho^2\right)E_{kz}^S &= 0. \end{aligned} \tag{39}$$

The set (39) gives exactly $\overleftrightarrow{\mathbf{D}}_0(\mathbf{k},\omega) . \mathbf{E}_k^S(\mathbf{k},\omega) = 0$, where $\mathbf{E}_k^S = \left(E_{k\rho}^S\widehat{\boldsymbol{\rho}}_k + E_{k\phi}^S\widehat{\boldsymbol{\phi}}_k + E_{kz}^S\widehat{\mathbf{z}}\right)$ is the electric field vector of the scattered wave. In a way, it is not surprising that the characteristics of the electric field of the scattered wave follow the same pattern as the incoming plane wave, as these waves are propagating in the same medium. The primary difference being that the scattered wave is represented by Hankel functions of the first kind, while the incoming wave is in terms of the Bessel function of the first kind. The former leading to an asymptotic form of an outgoing wave, while the latter being continuous at $\rho = 0$.

A non-trivial solution for the electric field components from (39) requires, as before, that $\det\left(\overleftrightarrow{\mathbf{D}}_0(\mathbf{k},\omega)\right) = 0$. Since n_{0z} is fixed by the incoming wave, the four solutions for n_ρ

follow from (12). However, only the two solutions corresponding to outgoing waves are kept; those solutions representing waves propagating towards the filament are discarded. If one of the solutions is imaginary then its counterpart is the complex conjugate. The wave root that corresponds to a decaying solution as a function of ρ is the one included in the analysis.

Let the two wave roots be denoted by $n_{\ell\rho}^S = ck_{\ell\rho}^S/\omega$ ($\ell = 1, 2$). Then, the electric field associated with the scattered waves takes on the form,

$$\begin{aligned}\mathbf{E}_S(\mathbf{r}) \;=\; \sum_{\ell=1}^{2}\sum_{m=-\infty}^{\infty} i^m\, \mathcal{E}_{\ell m}^S \Bigg[&\left\{ -iE_{\ell k\rho}^S \mathrm{H}_m^{(1)\prime}\left(k_{\ell\rho}^S\rho\right) - \frac{m}{\rho k_{\ell\rho}^S} E_{\ell k\phi}^S \mathrm{H}_m^{(1)}\left(k_{\ell\rho}^S\rho\right)\right\}\widehat{\boldsymbol{\rho}} + \\ &\left\{ -iE_{\ell k\phi}^S \mathrm{H}_m^{(1)\prime}\left(k_{\ell\rho}^S\rho\right) + \frac{m}{\rho k_{\ell\rho}^S} E_{\ell k\rho}^S \mathrm{H}_m^{(1)}\left(k_{\ell\rho}^S\rho\right)\right\}\widehat{\boldsymbol{\phi}} + \\ &E_{\ell kz}^S \mathrm{H}_m^{(1)}\left(k_{\ell\rho}^S\rho\right)\widehat{\mathbf{z}}\Bigg]\; e^{im\phi}\; e^{ik_{0z}z}. \end{aligned} \tag{40}$$

where the prime denotes the derivative with respect to the argument. The $\mathcal{E}_{\ell m}^S$ are constant coefficients, and the elements of the set $\left(E_{\ell k\rho}^S, E_{\ell k\phi}^S, E_{\ell kz}^S\right)$ are the polarization vectors equivalent to either (17) or (18).

IX. BOUNDARY CONDITIONS - DYNAMIC PROPERTIES

The magnetic fields associated with the incident wave, waves inside the filament, and the scattered waves can be derived from the corresponding electric fields using Faraday's equation,

$$\mathbf{B}(\mathbf{r}) \;=\; -\frac{i}{\omega}\nabla\times\mathbf{E}(\mathbf{r}). \tag{41}$$

Of the six boundary conditions (23) – (26), it can be shown that only four are independent (Appendix C). Choosing the four conditions as those given by Eqs. (25) and (26), it follows that the azimuthal and longitudinal components of the wave electric and magnetic fields are continuous at $\rho = a$ – the interface between the filament and the background plasma.

The azimuthal dependence of the m-th term in the series for the wave electric and magnetic fields, inside and outside the filament, is of the form $e^{im\phi}$. The orthogonality of these exponential functions implies that the m-th terms on the left and right-hand sides of (25)

and (26) have to be the same. Let

$$\alpha^I_{\phi m} = \frac{m}{k_{0\rho}a}\mathrm{J}_m\left(k_{0\rho}a\right)E_{0k\rho} - i\mathrm{J}'_m\left(k_{0\rho}a\right)E_{0k\phi}, \tag{42}$$

$$\alpha^S_{\phi\ell m} = \frac{m}{k^S_{\ell\rho}a}\mathrm{H}^{(1)}_m\left(k^S_{\ell\rho}a\right)E^S_{\ell k\rho} - i\mathrm{H}^{(1)\prime}_m\left(k^S_{\ell\rho}a\right)E^S_{\ell k\phi}, \tag{43}$$

$$\alpha^F_{\phi\ell m} = \frac{m}{k_{\ell\rho}a}\mathrm{J}_m\left(k_{\ell\rho}a\right)E_{\ell k\rho} - i\mathrm{J}\prime_m\left(k_{\ell\rho}a\right)E_{\ell k\phi}, \tag{44}$$

$$\beta^I_{\phi m} = k_{0z}\mathrm{J}'_m\left(k_{0\rho}a\right)E_{0k\rho} - i\frac{mk_{0z}}{k_{0\rho}a}\mathrm{J}_m\left(k_{0\rho}a\right)E_{0k\phi} - k_{0\rho}\mathrm{J}'_m\left(k_{0\rho}a\right)E_{0kz}, \tag{45}$$

$$\beta^S_{\phi\ell m} = k_{0z}\mathrm{H}^{(1)\prime}_m\left(k^S_{\ell\rho}a\right)E^S_{\ell k\rho} - i\frac{mk_{0z}}{k^S_{\ell\rho}a}\mathrm{H}^{(1)}_m\left(k^S_{\ell\rho}a\right)E^S_{\ell k\phi} - k^S_{\ell\rho}\mathrm{H}^{(1)\prime}_m\left(k^S_{\ell\rho}a\right)E^S_{\ell kz}, \tag{46}$$

$$\beta^F_{\phi\ell m} = k_{0z}\mathrm{J}'_m\left(k_{\ell\rho}a\right)E_{\ell k\rho} - i\frac{mk_{0z}}{k_{\ell\rho}a}\mathrm{J}_m\left(k_{\ell\rho}a\right)E_{\ell k\phi} - k_{\ell\rho}\mathrm{J}'_m\left(k_{\ell\rho}a\right)E_{\ell kz}, \tag{47}$$

$$\alpha^I_{zm} = \mathrm{J}_m\left(k_{0\rho}a\right)E_{0kz}, \tag{48}$$

$$\alpha^S_{z\ell m} = \mathrm{H}^{(1)}_m\left(k^S_{\ell\rho}a\right)E^S_{\ell kz}, \tag{49}$$

$$\alpha^F_{z\ell m} = \mathrm{J}_m\left(k_{\ell\rho}a\right)E_{\ell kz}, \tag{50}$$

$$\beta^I_{zm} = ik_{0\rho}\mathrm{J}_m\left(k_{0\rho}a\right)E_{0k\phi}, \tag{51}$$

$$\beta^S_{z\ell m} = ik^S_{\ell\rho}\mathrm{H}^{(1)}_m\left(k^S_{\ell\rho}a\right)E^S_{\ell k\phi}, \tag{52}$$

$$\beta^F_{z\ell m} = ik_{\ell\rho}\mathrm{J}_m\left(k_{\ell\rho}a\right)E_{\ell k\phi}, \tag{53}$$

where the superscripts I, S, and F refer to incident wave, scattered wave, and waves inside the filament, respectively, and $\ell = 1, 2$. The α's and β's defined above are functions of the plasma parameters and are completely known once these parameters are specified. From the continuity conditions (25) and (26), it follows that

$$\alpha^F_{\phi 1m}\mathcal{E}_{1m} + \alpha^F_{\phi 2m}\mathcal{E}_{2m} - \alpha^S_{\phi 1m}\mathcal{E}^S_{1m} - \alpha^S_{\phi 2m}\mathcal{E}^S_{2m} = \alpha^I_{\phi m}\mathcal{E}_0, \tag{54}$$

$$\alpha^F_{z1m}\mathcal{E}_{1m} + \alpha^F_{z2m}\mathcal{E}_{2m} - \alpha^S_{z1m}\mathcal{E}^S_{1m} - \alpha^S_{z2m}\mathcal{E}^S_{2m} = \alpha^I_{zm}\mathcal{E}_0, \tag{55}$$

$$\beta^F_{\phi 1m}\mathcal{E}_{1m} + \beta^F_{\phi 2m}\mathcal{E}_{2m} - \beta^S_{\phi 1m}\mathcal{E}^S_{1m} - \beta^S_{\phi 2m}\mathcal{E}^S_{2m} = \beta^I_{\phi m}\mathcal{E}_0, \tag{56}$$

$$\beta^F_{z1m}\mathcal{E}_{1m} + \beta^F_{z2m}\mathcal{E}_{2m} - \beta^S_{z1m}\mathcal{E}^S_{1m} - \beta^S_{z2m}\mathcal{E}^S_{2m} = \beta^I_{zm}\mathcal{E}_0. \tag{57}$$

For each azimuthal mode number m, these four linear equations can be solved for the amplitudes $\mathcal{E}_{1m}$, $\mathcal{E}_{2m}$ for the wave fields inside the filament, and $\mathcal{E}^S_{1m}$, $\mathcal{E}^S_{2m}$ for the scattered wave fields. These amplitudes are expressed in terms of the wave amplitude of the incoming wave $\mathcal{E}_0$. Since the entire scattering model is linear, without any loss of generality, all the wave amplitudes can be normalized to $\mathcal{E}_0$. Given these amplitudes, it is straightforward to

construct the full wave electromagnetic fields inside the filament using (35), and outside the filament using (22) and (40).

It is interesting to compare the model for the scattering of RF waves by cylindrical filaments with the scattering by spherical blobs. In the former case, the amplitude equations (54)–(57) are for a single azimuthal mode. While, in the latter case, the amplitude equations couple different azimuthal modes [14, 15]. Numerically, the scattering off spherical blobs is more challenging. The scattering off blobs is three-dimensional while that off filaments is two-dimensional – a direct consequence of the kinematic property of the boundary conditions.

This completes the model for the scattering of RF waves in a plasma by a cylindrical filament with its axis aligned along the magnetic field line.

X. RESULTS AND DISCUSSION

We illustrate the scattering of RF waves by a filament for some typical plasma parameters. The aim is to provide physical insight into the scattering process and not get caught up with the details of the plasma that may exist in the scrape-off layer in a fusion device. The incoming RF plane wave is assumed to be either an electron cyclotron wave or a lower hybrid wave.

Some of the features that result from the scattering model can be best displayed by the time-averaged Poynting vector [19],

$$\langle \mathbf{S}\,(t) \rangle \;=\; \frac{1}{2} \mathrm{Re}\,(\mathbf{E} \times \mathbf{H}^{*})\,, \tag{58}$$

where $< \ldots >$ denotes the time average, and $\mathbf{H}^{*}$ is the complex conjugate of the magnetic intensity $\mathbf{H}$. In a plasma, the wave magnetic field $\mathbf{B}$ is related to $\mathbf{H}$ by $\mathbf{B} = \mu_0 \mathbf{H}$, where μ_0 is the free-space permeability. In the numerical calculations, it is more appropriate to quantify the normalized Poynting vector

$$\mathbf{P} \;=\; \frac{\langle \mathbf{S}\,(t) \rangle}{|\,\langle \mathbf{S}_I \rangle\,|}, \tag{59}$$

where $|\,\langle \mathbf{S}_I \rangle\,|$ is the magnitude of the time-averaged Poynting vector of the incident plane wave.

A. Electron cyclotron waves

The results that follow are for a plasma composed of electrons and deutrons, in a magnetic field $B_0 = 4.5$ T. The incident RF wave has a frequency of 170 GHz and is assumed to be propagating normal to the direction of the magnetic field, i.e., $n_{oz} = 0$. The phase ϕ_k in (22) is set to zero so that the incident wave is propagating along the positive x-direction.

Figure 2 shows the real part of the four roots of the perpendicular wave number $\mathrm{Re}\,(n_\rho)$ as a function of the electron density n_e. The solid lines represent the dispersion characteristics of the ordinary, or O, wave while the dashed line is that for the extraordinary, or X, wave. The radial index of refraction n_ρ is imaginary in the regions where $\mathrm{Re}\,(n_\rho) = 0$. The O wave has a cutoff near $n_e \approx 3.58 \times 10^{20}$ m^{-3}, while the X wave has two cutoffs near $n_e \approx 9.29 \times 10^{19}$ m^{-3} and $n_e \approx 6.24 \times 10^{20}$ m^{-3}. The X wave also has a resonance, the upper hybrid resonance [18], near $n_e \approx 1.62 \times 10^{20}$ m^{-3}.

1. Low density plasma

The electron density of the background plasma and of the plasma inside the filament is taken to be $n_{eb} = 2 \times 10^{18}$ m^{-3} and $n_{ef} = 2.5 \times 10^{18}$ m^{-3}, respectively, which implies that $\delta n = 0.25$. The radial wave numbers for the scattered waves $n_{1\rho}^S = 0.9972$ and $n_{2\rho}^S = 0.9938$ correspond to the O wave and the X wave, respectively. Inside the filament $n_{1\rho} = 0.9965$ and $n_{2\rho} = 0.9922$ for the O wave and X wave, respectively.

Let the incident plane wave be an O wave so that $n_{0\rho} = n_{1\rho}^S$. For $n_{0z} = 0$, only the E_{0kz} component of the wave electric field is non-zero. Consequently, the Cartesian components of the Poynting vector for the incoming wave are, $P_x^I = 1$, $P_y^I = 0$, and $P_z^I = 0$. The x-direction is directed towards the core of the toroidal plasma and the y-component is along the poloidal direction.

Figure 3 shows the contour plot for P_x in the $x - y$ plane. The filament has a radius $a = 1$ cm, centered at $x = y = 0$, with its cross-section displayed as a white circle. The O wave is incident from the left-hand side ($x < 0$). Since P_x is positive, the power flow is in the positive x-direction. The uniformity in the spatial region $x < 0$ indicates that there is no backscattering of the incident wave due to the filament. The scattering in the forward direction, and the power flowing into the plasma, is not spatially uniform in the

y-direction, which would have been the case if the filament did not exist. However, the spatial redistribution of power along the y-axis is small as indicated by the scale on the right-hand side of Fig. 3.

If, instead, the incident wave is the X wave with $n_{0\rho} = n_{2\rho}^S$, the results (not shown) are similar to those shown in Fig. 3 for the O wave. The scattering is in the forward direction with essentially no reflected power from the filament.

Figure 4 is a comparison of P_x as a function of y, in the wake of the filament at $x = 2$ cm, for an incident O wave (solid line) and X wave (dashed line). The non-uniformity in the x-component of the Poynting vector is due to diffraction, and constructive and destructive interference between the incident and scattered waves. This leads to shadowing, where P_x falls below 1, and focusing, where P_x is greater than 1. The shadowing and focusing is more noticeable for an incident X wave when compared to the O wave. However, the maximum effect is limited to within 5%.

For either case of the incident plane wave, at $x = -2$ cm, in the region of backscattering, P_x is essentially 1 (to within 0.02%) as a function of y, thereby indicating that there is no reflection of the waves by the filament.

If the density inside the filament is increased, the shadowing and focusing effects are more pronounced. Figure 5 shows the results for an incident O wave (solid line) and X wave (dashed line) when the density inside the filament is 3.7×10^{18} m^{-3}. In this case, $\delta n = 0.85$ and, inside the filament, $n_{1\rho} = 0.9948$ and $n_{2\rho} = 0.9883$ for the O wave and X wave, respectively. Comparing Fig. 5 with Fig. 4 shows that an increase in δn enhances the effect of shadowing and focusing, leading to a larger variation in the spatial profile of the electron cyclotron waves propagating towards the core of a tokamak plasma.

2. High density plasma – effect of a wave cutoff

Consider a filament with density $n_{ef} = 3.71 \times 10^{20}$ m^{-3} embedded in a background plasma with density $n_{eb} = 3.4 \times 10^{20}$ m^{-3}. For these densities, as seen in Fig. 2, the O wave does not propagate inside the filament. The radial wave numbers of the scattered O and X waves are $n_{1\rho}^S = 0.227$ and $n_{2\rho}^S = 1.048$, respectively. Inside the filament $n_{1\rho} = 0.188i$ for the O wave and $n_{2\rho} = 0.968$ for the X wave.

It can be easily shown from Eqs. (17) and (18), that the Cartesian components of the

Poynting vector for either of the incoming waves, O wave or X wave, are $P_x^I = 1$, $P_y^I = 0$, and $P_z^I = 0$.

Figures 6 and 7 display P_x and P_y, respectively, in the $x-y$ plane for an incident O wave. The filament blocks the O wave from propagating through it, leading to a shadow in the wake of the filament. There is a focusing effect in the forward direction, as evidenced by spatial regions of enhanced Poynting flux away from the shadow. The existence of diffraction-type patterns, due to interference between the incident and scattered waves in the front of the filament ($x < 0$), is a clear indication of backscattering, or reflection of waves, by the filament. Moreover, as seen in Fig. 7, there is enhanced side-scattering with the Poynting flux in the positive and negative y-directions; the flux being symmetric about the y-axis.

In contrast, as seen in Figs. 8 and 9, for an incident X wave, there is little or no backscattering. The dominant scattering is in the forward direction with some side-scattering. The differences between an incident O wave and X wave are illustrated in Figs. 10 and 11. The shadow region created in the forward direction (Fig. 10), in the wake of the filament, is prominently displayed for an incident O wave; the Poynting flux is appreciably enhanced for the incident X wave. Figure 11 shows a large variation in the Poynting flux of the O wave in the front of the filament due to backscattering; there being essentially no backscattering of the X wave.

A comparison between Fig. 7 and Fig. 9 indicates that the O wave does not propagate inside the filament while the X wave does. The differences in the overall scattering patterns between the two incident waves can be attributed to the dissimilarities in the wave fields inside the filament. The connection between the fields inside and outside the filament being through the boundary conditions.

In the vicinity of the filament, the side-scattered Poynting flux in the forward and backward regions, as displayed in Figs. 12 and 13, respectively, is spatially structured in space. Figure 13 shows that the O mode undergoes backscattering while the X mode does not.

B. Lower hybrid waves

The effect of a filament on the propagation of waves in the lower hybrid range of frequencies is discussed in this section. As for electron cyclotron waves, the plasma is assumed to be made up of electrons and deutrons confined in a magnetic field of 4.5 T. The incident

wave has a frequency of 4.6 GHz with $n_{oz} = 2$. Without loss of generality, the phase ϕ_k in (22) is set to zero, so that the incident wave vector is in the $x - z$ plane.

Figure 14 shows the $\mathrm{Re}\,(n_\rho)$, for the four roots of the dispersion relation, as a function of n_e. The solid lines represent the dispersion characteristics of the slow lower hybrid waves, while the dashed line is that for the fast waves. For $n_e \lesssim 2.09 \times 10^{20}$ m^{-3}, the perpendicular wave number for the fast wave is purely imaginary, indicating the region in which the wave is evanescent.

1. Low density plasma

As in the case of electron cyclotron waves in a low density plasma, the electron density of the background plasma and of the plasma inside the filament is taken to be $n_{eb} = 2 \times 10^{18}$ m^{-3} and $n_{ef} = 2.5 \times 10^{18}$ m^{-3}, respectively. For these densities, the slow wave is the only propagating wave; the fast wave is evanescent everywhere. The radial wave numbers for the scattered waves are $n^S_{1\rho} = 4.423$ and $n^S_{2\rho} = 1.725i$ for the slow and fast waves, respectively, and inside the filament $n_{1\rho} = 5.01$ and $n_{2\rho} = 1.722i$, respectively.

In the lower hybrid range of frequencies, the slow wave is a backward wave [18]; the group velocity of the wave is in a direction opposite to the phase velocity. Thus, in order to have the Poynting flux directed toward the positive x-direction, the appropriate choice for an incident slow wave is $n_{0\rho} = -4.423$. The normalized Cartesian components of the Poynting vector for the incident plane wave are, $P^I_x \approx 0.32$, $P^I_y = 0$, and $P^I_z \approx 0.95$.

Figure 15 shows the effect of the filament on P_x in the $x - y$ plane. While the power flow is in the positive x-direction, the diffraction pattern, due to the phase mixing of the incident and scattered waves, is directed towards the negative x-direction. This is a consequence of the backward nature of the slow wave [18]. The power flow is along the direction of the group velocity. Figure 16 is a plot of P_x as a function of y at $x = 2$ cm in the wake of the filament (solid line), and at $x = -2$ cm in front of the filament (dashed line). In the forward direction P_x is close to P^I_x while in the backward direction there is spatial redistribution of power with enhanced Poynting flux in the vicinity of the x-axis. There is constructive interference between the incident and scattered waves along the negative x-axis, and destructive interference away from the x-axis in the region near $y \approx \pm 1.5$ cm. The contour plot of P_z in Fig. 17 shows features similar to Fig. 15 for the backscattered fields;

the forward scattering, unlike in Figs. 15 and 16, develops an interference pattern due to the combined fields of the incident and scattered waves. Figure 17 shows an enhanced P_z inside the filament, indicating power flow in the axial direction. The filament almost behaves like a transmission line with power flowing in its interior.

Besides affecting P_x and P_z, the principal components of the Poynting vector of the incident plane wave, the filament also leads to side-scattering as seen in Fig. 18. The cumulative affect of the filament is to change the spatial structure of the slow lower hybrid wave propagating into the core of the plasma, as well as scatter power back in the direction of the incoming plane wave.

2. High density plasma with density depleted filament

The final set of results is to demonstrate the effect of the filament when the density inside the filament is less than the background density. It is also illustrative of the role that the filament plays in the scattering process even when the wavelength of the incident wave is much larger than the transverse dimension of the filament.

Let the electron density of the background plasma and of the plasma inside the filament be $n_{eb} = 2.2 \times 10^{19}$ m^{-3} and $n_{ef} = 1.9 \times 10^{19}$ m^{-3}, respectively. The dispersion relation in Fig. 14 shows that only the slow lower hybrid wave can propagate inside the filament, while both the slow and fast waves can propagate in the background plasma. For these parameters, the radial wave numbers for the scattered slow and fast waves are $n_{1\rho}^S = 14.475$ and $n_{2\rho}^S = 0.578$, respectively. Inside the filament, the radial wave numbers are $n_{1\rho} = 13.599$ and $n_{2\rho} = 0.742i$, respectively. The corresponding wavelengths in the background plasma are $\lambda_{1\rho}^S = 2\pi c/\left(n_{1\rho}\omega\right) = 0.45$ cm and $\lambda_{2\rho}^S = 11.28$ cm. Inside the filament, the wavelength of the slow wave is $\lambda_{1\rho} = 0.48$ cm.

Let the incident plane wave be the fast lower hybrid wave with $n_{0\rho} = 0.578$. The wavelength of the wave, 11.28 cm, is much longer than the radius, $a = 1$ cm, of the filament. The components of the Poynting vector for the incident wave are, $P_x^I = 0.127$, $P_y^I = 0$, and $P_z^I = 0.992$. Figure 19 is a contour plot of P_x in the vicinity of the filament. It is noteworthy that the filament acts like an antenna radiating circular waves in the $x - y$ plane. The incident fast wave has coupled power to the only mode that propagates inside the filament – the slow wave. The fields inside the filament, in turn, affect the scattered field so that P_x

has the pattern seen in Fig. 19. In order to capture the effect of the filament on a scale that is representative of the wavelength of the incoming fast wave, a spatially extended view of the scattering contours is displayed in Fig. 20. The filament leads to regions of enhanced and depleted Poynting flux as the scattered waves emanating from the filament interfere, constructively and destructively, with the incident field.

The incident fast wave induces charge oscillations inside the filament. These charge oscillations induce internal waves that are consistent with the plasma permittivity inside the filament, and with its boundary. Hence, the oscillations inside the filament are the short wavelength, slow lower hybrid waves and the wave patterns are essentially concentric circles. This is an interesting result given the fact that the radial wavelength of the incident wave is much longer than the radius of the filament. For such a disparity in radial scales, it would seem that the filament has little or no affect on the propagation of the incident wave. Clearly, this is not the case.

It is important to note that the fast wave, unlike the slow wave, is a forward wave. Hence, the diffraction pattern is in the forward direction. However, since the slow wave excited by the filament is a backward wave, the pattern, unlike for electron cyclotron waves, originates from the front of the filament which faces the incoming wave.

XI. CONCLUSIONS

Density fluctuations and coherent structures, like blobs, are ubiquitous in the scrape-off layer in the edge region of a tokamak plasma. RF waves, excited by antennas or waveguides, have to propagate through this region on their way to the core of the plasma. Since RF waves are the mainstay for heating fusion plasmas and for generating plasma currents, it is desirable to understand the effect of fluctuations on the propagation characteristics of the waves. The variation in the fluctuations, relative to the background plasma density, is large enough that geometric optics is not an appropriate description for studying their effect on RF waves. This is particularly true for the propagation of RF waves through coherent fluctuations, like blobs and filaments.

In this paper, a full-wave theoretical model has been developed for describing the scattering of plane RF waves by a cylindrical filament embedded in an ambient, magnetized plasmas. The plasma inside and outside the filament is assumed to be cold and homoge-

neous; however, the density difference between the two regions is completely arbitrary and not limited by the approximations necessary for applying geometric optics.

The spatial structure of the electric and magnetic fields is given by the Faraday-Ampere equation, which has the same form as the vector Helmholtz equation. Mathematical techniques developed for Mie scattering [12, 13], and scattering of RF waves by spherical blobs [14, 15], are used to solve the partial differential equation and determine the electric and magnetic fields inside and outside the filament.

The cold plasma supports two independent plasma waves that satisfy the appropriate dispersion relation [18]. The incident RF wave is one of these two plasma waves. The wave modes excited inside the filament, by the RF wave, are a linear combination of the two cold plasma waves satisfying the dispersion relation inside the filament. These wave modes propagate in all directions relative to the direction of the magnetic field, and, in turn, lead to wave modes outside the filament that are a linear combination of the cold plasma waves in the background plasma. The wave modes outside the filament similarly propagate in all directions. The self-consistent form of the wave fields is obtained by enforcing the boundary conditions at the interface between the filament and the background plasma. Since the scattered fields propagate in all directions, there is forward scattering in the wake of the filament, backward scattering, or reflection, in front of the filament towards the incoming plane wave, and side-scattering leading to surface waves. These features are similar to those associated with the scattering of RF waves by spherical blobs [14, 15].

There are two striking differences between scattering by a spherical blob [14, 15] and by a cylindrical filament. First, the former leads to the spreading of the parallel (to the magnetic field) component of the wave vector, while the latter preserves the parallel component, keeping it the same as that of the incident plane wave. Thus, scattering from a blob leads to a broadening of the spectrum for the wave propagating towards the core of the plasma. Second, the fields reconstitute in the wake of blob but not in the wake of the filament. Consequently, there is considerable spatial structure in the Poynting flux directed towards the core of the plasma when scattering off a filament.

For a filament of finite axial extent, the formulation has to be modified in the following way. The Fourier transform in k_z in (27) has to be replaced by a finite Fourier transform. For a filament of length L located in the interval $z \in [-L/2, L/2]$, the electric field takes on

the form

$$\mathbf{E}_F\left(\mathbf{r}\right) \;=\; \int_0^\infty dk_\rho \; k_\rho \; \int_0^{2\pi} d\phi_k \; \int_{-L/2}^{L/2} dk_z \; \mathbf{E}_F\left(\mathbf{k}\right) e^{ik_\rho \rho \cos(\phi - \phi_k)} e^{ik_z z}, \tag{60}$$

that has to be substituted in the Faraday-Ampere equation (2). Unlike for an infinitely extended filament, k_z is not the same as for the incident plane wave. It is determined by the boundary conditions at the ends of the filament $z = \pm L/2$,

$$\widehat{\mathbf{z}}.\left(\mathbf{D}_I + \mathbf{D}_S\right)\Big|_{z=\pm L/2} \;=\; \widehat{\mathbf{z}}.\,\mathbf{D}_F\Big|_{z=\pm L/2}, \tag{61}$$

$$\widehat{\mathbf{z}}.\left(\mathbf{B}_I + \mathbf{B}_S\right)\Big|_{z=\pm L/2} \;=\; \widehat{\mathbf{z}}.\,\mathbf{B}_F\Big|_{z=\pm L/2}, \tag{62}$$

$$\widehat{\mathbf{z}} \times \left(\mathbf{E}_I + \mathbf{E}_S\right)\Big|_{z=\pm L/2} \;=\; \widehat{\mathbf{z}} \times \mathbf{E}_F\Big|_{z=\pm L/2}, \tag{63}$$

$$\widehat{\mathbf{z}} \times \left(\mathbf{B}_I + \mathbf{B}_S\right)\Big|_{z=\pm L/2} \;=\; \widehat{\mathbf{z}} \times \mathbf{B}_F\Big|_{z=\pm L/2}. \tag{64}$$

These boundary conditions, which are in addition to those in equations (23)-(26), determine the range of k_z excited inside the finite filament, and, importantly, the spectrum of k_z in the scattered field. It is to be expected that, similar to the scattering by a spherical blob, a finite cylindrical filament will lead to a spreading of the parallel component of the wave vector. As noted in the introduction section of this paper, the theoretical modeling of scattering by a finite filament is a topic for a separate paper.

In low density plasmas, electron cyclotron waves are scattered in the forward direction by the filament irrespective of an incident O wave or X wave. The component of the Poynting vector, representing power flow, directed towards the core of the plasma is spatially structured due to diffraction. The interference between the incident and scattered fields leads to regions of enhanced power flow, due to focusing of the fields, and depleted power flow, due to shadowing behind the filament. The spatial variations in the power flow increases as the density inside the filament is increased relative to the background density. There is essentially no side-scattering or backscattering of the electron cyclotron waves. In a high density plasma when the O wave does not propagate inside the filament, the scattering of incident O and X waves is quite different. For the O wave, the shadowing and focusing effects are prominent in the wake of the filament. This is accompanied by backscattering and side-scattering. The filament acts as a barrier with no discernible wave activity inside the filament. For an incident X wave, forward scattering is dominant, with some side-scattering and negligible backscattering. There are regions of substantially enhanced Poynting flux, or

electric fields in the forward direction. The X waves also propagate in the interior of the filament which help reduce the effect of shadowing when compared with an incident O wave.

Some of the features associated with the scattering of lower hybrid waves by a filament are in stark contrast to the results for the electron cyclotron waves. In a low density plasmas, in which only the slow wave is propagating, the backscattering of the wave is prominent. The diffraction pattern, formed by the incident wave and the scattered waves, is in the backward direction even though the Poynting flux is the forward direction. This is a consequence of the backward wave characteristic of the slow wave – the group velocity of the wave is in a direction opposite to the phase velocity. Regions of large electric fields occur near the boundary layer separating the filament from the background plasma. Inside the filament, power flows along the magnetic field line – the filament behaves like a transmission line. The diffraction patterns also exist in the forward direction.

The linear coupling of power from one cold plasma wave, excited by an external source, to the other cold plasma wave is a natural consequence of the scattering process by the filament. This is illustrated by considering lower hybrid wave scattering in a high density plasma. An incident fast wave, with its radial wavelength much larger than the radial dimension of the filament, excites, within the filament, a slow wave, with a much shorter wavelength than the fast wave. The filament behaves like an antenna and excites a slow wave in the background plasma showing linear conversion of power from the fast wave to the slow wave.

The scattering of RF waves by arbitrary shaped density fluctuations, with inhomogeneous density profiles, will require a completely numerical approach. The theory developed in this paper can be used as a check of these, more general, simulation codes.

XII. ACKNOWLEDGEMENTS

AKR is supported by the US Department of Energy Grant numbers DE-FG02-91ER-54109, DE-FG02-99ER-54525-NSTX, and DE-FC02-01ER54648. KH is supported in part by ER Project CfP-WP14-ER-01/Swiss Confederation-03 titled "Radio frequency wave propagation and absorption in toroidally magnetized plasmas: Scattering by turbulent structures and quasilinear effects," and in part by the National Programme on Controlled Thermonuclear Fusion associated with the EUROfusion Consortium in the framework of EJP Co-fund Action, Number SEP-210130335.

Appendix A CYLINDRICAL COORDINATE SYSTEM

The rotation matrix transforming the Cartesian coordinate system $(\widehat{\mathbf{x}}, \widehat{\mathbf{y}}, \widehat{\mathbf{z}})$ to the spatial cylindrical coordinate system $\left(\widehat{\boldsymbol{\rho}}, \widehat{\boldsymbol{\phi}}, \widehat{\mathbf{z}}\right)$ is,

$$\overleftrightarrow{\mathcal{R}}_{\rho} \;=\; \begin{pmatrix} \cos\phi & -\sin\phi & 0 \\ \sin\phi & \cos\phi & 0 \\ 0 & 0 & 1 \end{pmatrix}, \tag{65}$$

where ϕ is the angle between the position vector $\mathbf{r}$ and the x-axis.

The rotation matrix transforming the Cartesian coordinate system to the wave vector cylindrical coordinate system $\left(\widehat{\boldsymbol{\rho}}_k, \widehat{\boldsymbol{\phi}}_k, \widehat{\mathbf{z}}\right)$ is,

$$\overleftrightarrow{\mathcal{R}}_{k} \;=\; \begin{pmatrix} \cos\phi_k & -\sin\phi_k & 0 \\ \sin\phi_k & \cos\phi_k & 0 \\ 0 & 0 & 1 \end{pmatrix}, \tag{66}$$

where ϕ_k is the angle between the wave vector $\mathbf{k}$ and the x-axis.

It is easy to show that $\overleftrightarrow{\mathcal{R}}_{\rho}.\overleftrightarrow{\mathbf{K}}.\overleftrightarrow{\mathcal{R}}_{\rho}^{-1} = \overleftrightarrow{\mathbf{K}}$ and $\overleftrightarrow{\mathcal{R}}_{k}.\overleftrightarrow{\mathbf{K}}.\overleftrightarrow{\mathcal{R}}_{k}^{-1} = \overleftrightarrow{\mathbf{K}}$, where $\overleftrightarrow{\mathbf{K}}$ is the permittivity tensor in (3).

Appendix B VECTOR CYLINDER FUNCTIONS

The Faraday-Ampere equation (2) is of the form of a vector Helmholtz equation. The solutions to a vector Helmholtz equation can be constructed from the scalar Helmholtz equation

$$\nabla^2\psi\left(\mathbf{r}\right) \;+\; k^2\,\psi\left(\mathbf{r}\right) \;=\; 0, \tag{67}$$

using the procedure described in [19]. Here $k^2 = \mathbf{k}.\mathbf{k}$ is assumed to be a constant and ψ is a scalar field that is a function of the position vector $\mathbf{r}$. The solution to (67) is obtained by separation of variables [19],

$$\psi\left(\mathbf{r}\right) \;=\; \sum_{m=-\infty}^{\infty} c_m\psi_m \;\equiv\; \sum_{m=-\infty}^{\infty} c_m\mathcal{Z}_m\left(k_\rho\rho\right)e^{ik_z z+im\phi}, \tag{68}$$

where c_m is a constant for all m, $\mathcal{Z}_m$ represents either Bessel functions or Hankel functions of order m [21], $k_z = \mathbf{k}.\widehat{\mathbf{z}}$, $k_\rho = |\mathbf{k} - k_z\widehat{\mathbf{z}}|$, and ϕ is the azimuthal angle. The Bessel and Hankel functions can be of the first or second kind [21].

The vector cylinder function are then obtained from (68) as follows [19].

$$\begin{aligned}
\mathbf{l}_m(\rho,\phi,z;k_\rho,k_z) &= \nabla\psi_m = \left[\left(\frac{\partial}{\partial\rho}\mathcal{Z}_m\right)\widehat{\boldsymbol{\rho}} + \left\{\frac{im}{\rho}\widehat{\boldsymbol{\phi}} + ik_z\,\widehat{\mathbf{z}}\right\}\mathcal{Z}_m\right]e^{ik_z z+im\phi},\\
\mathbf{m}_m(\rho,\phi,z;k_\rho,k_z) &= \nabla\times(\psi_m\widehat{\mathbf{z}}) = \left[\frac{im}{\rho}\mathcal{Z}_m\,\widehat{\boldsymbol{\rho}} - \left(\frac{\partial}{\partial\rho}\mathcal{Z}_m\right)\widehat{\boldsymbol{\phi}}\right]e^{ik_z z+im\phi}, \qquad (69)\\
\mathbf{n}_m(\rho,\phi,z;k_\rho,k_z) &= \frac{1}{k}\nabla\times\mathbf{m}_m = \left[\frac{ik_z}{k}\left(\frac{\partial}{\partial\rho}\mathcal{Z}_m\right)\widehat{\boldsymbol{\rho}} - \left\{\frac{k_z}{k}\frac{m}{\rho}\widehat{\boldsymbol{\phi}} - \frac{k_\rho^2}{k}\widehat{\mathbf{z}}\right\}\mathcal{Z}_m\right]e^{ik_z z+im\phi}.
\end{aligned}$$

The argument of the $\mathcal{Z}$ functions is $k_\rho\rho$

The vector cylinder functions are such that $\nabla\times\mathbf{l}_m = 0$, $\nabla\times\mathbf{m}_m = k\mathbf{n}_m$, and $\nabla\times\mathbf{n}_m = k\mathbf{m}_m$. Thus, $\mathbf{l}_m$ represents a purely longitudinal electromagnetic wave. Such waves do not exist in vacuum, but can exist in plasmas.

Some additional properties are: $\nabla.\mathbf{m}_m = 0$, $\nabla.\mathbf{n}_m = 0$, $\nabla\times(\nabla\times\mathbf{l}_m) = 0$, $\nabla\times(\nabla\times\mathbf{m}_m) = k^2\mathbf{m}_m$, and $\nabla\times(\nabla\times\mathbf{n}_m) = k^2\mathbf{n}_m$.

The vector cylinder functions do not form an orthogonal set [19]. However, they form a complete set [19, 20] – a property that is important for constructing the electromagnetic fields of the scattered waves.

Appendix C INDEPENDENT BOUNDARY CONDITIONS

Of the six boundary conditions Eqs. (23) – (26) only four are independent. The four boundary conditions that follow from Eqs. (25) and (26) have been imposed at the interface $\rho = a$ in order to complete the formulation of the scattering theory. In this section, it is shown that the other two boundary conditions, given by Eqs. (23) and (24), follow from these four equations.

Since there is no coupling between different azimuthal modes, each term in the summation over m can be treated independently. Consider the expression for the incoming plane wave given by Eq. (22). For a given m, the electric and magnetic field vectors of the wave are, respectively,

$$\mathbf{E}_I^{(m)} = \left(-iE_{0k\rho}\mathrm{J}'_m - \frac{m}{\rho k_{0\rho}}E_{0k\phi}\mathrm{J}_m\right)\widehat{\boldsymbol{\rho}} + \left(-iE_{0k\phi}\mathrm{J}'_m + \frac{m}{\rho k_{0\rho}}E_{0k\rho}\mathrm{J}_m\right)\widehat{\boldsymbol{\phi}} + E_{0kz}\mathrm{J}_m\widehat{\mathbf{z}}, \quad (70)$$

$$\mathbf{B}_I^{(m)} = \left(-i\frac{m}{\rho k_{0\rho}}k_{0z}E_{0k\rho}\mathrm{J}_m - k_{0z}E_{0k\phi}\mathrm{J}'_m + \frac{im}{\rho}E_{0kz}\mathrm{J}_m\right)\widehat{\boldsymbol{\rho}} + \left(k_{0z}E_{0k\rho}\mathrm{J}'_m - \frac{im}{\rho k_{0\rho}}k_{0z}E_{0k\phi}\mathrm{J}_m - k_{0\rho}E_{0kz}\mathrm{J}'_m\right)\widehat{\boldsymbol{\phi}} + ik_{0\rho}E_{0k\phi}\mathrm{J}_m\widehat{\mathbf{z}}, \quad (71)$$

where the terms $\mathcal{E}_0$, $e^{im(\phi-\phi_k)}$, $e^{ik_{0z}z}$, and $-i/\omega$ have been factored out. These terms do not affect the discussion that follows. The expression for the magnetic field (71) is obtained from (70) using Faraday's equation (41).

The four terms that are part of the left-hand side of Eqs. (25) and (26) follow from (70) and (71),

$$\frac{m}{\rho k_{0\rho}}E_{0k\rho}\mathrm{J}_m - iE_{0k\phi}\mathrm{J}'_m, \quad (72)$$

$$-E_{0kz}\mathrm{J}_m, \quad (73)$$

$$k_{0z}E_{0k\rho}\mathrm{J}'_m - \frac{im}{\rho k_{0\rho}}k_{0z}E_{0k\phi}\mathrm{J}_m - k_{0\rho}E_{0kz}\mathrm{J}'_m, \quad (74)$$

$$-ik_{0\rho}E_{0k\phi}\mathrm{J}_m. \quad (75)$$

The contribution to the left-hand side of (24) from the incident wave is,

$$-i\frac{m}{\rho k_{0\rho}}k_{0z}E_{0k\rho}\mathrm{J}_m - k_{0z}E_{0k\phi}\mathrm{J}'_m + \frac{im}{\rho}E_{0kz}\mathrm{J}_m. \quad (76)$$

This form can be easily obtained from (72) and (73), by multiplying the terms in (72) and (73) by $-ik_{0z}$ and im/ρ, respectively, and adding the resulting expressions. Since k_{0z} is a constant, $\rho = a$ at the boundary, and each azimuthal mode m is independent, the multipliers are constants. Hence, for the incoming wave, the expression on the left-hand side of (24) is a linear combination of the two expressions obtained from the left-hand side of (25).

Since $\mathbf{D} = \epsilon_0 \overleftrightarrow{\mathbf{K}}.\mathbf{E}$, the contribution of the incoming wave to the left-hand side of (23) is,

$$K_\rho\left(-iE_{0k\rho}\mathrm{J}'_m - \frac{m}{\rho k_{0\rho}}E_{0k\phi}\mathrm{J}_m\right) - iK_\phi\left(-iE_{0k\phi}\mathrm{J}'_m + \frac{m}{\rho k_{0\rho}}E_{0k\rho}\mathrm{J}_m\right), \quad (77)$$

where the multiplier ϵ_0 has been factored out. From the polarization equation $\overleftrightarrow{\mathbf{D}}.\mathbf{E} = 0$, it follows that,

$$K_\rho E_{0k\rho} = n_{0z}^2 E_{0k\rho} + iK_\phi E_{0k\phi} - n_{0\rho}n_{0z}E_{0kz}, \quad (78)$$

$$K_\rho E_{0k\phi} = -iK_\phi E_{0k\rho} + n_{0\rho}^2 E_{0k\phi}. \quad (79)$$

Substituting (78) and (79) in (77) yields,

$$\frac{c^2}{\omega^2}\left\{-ik_{0z}^2E_{0k\rho}\mathrm{J}_m + ik_{0\rho}k_{0z}E_{0kz}\mathrm{J}'_m - \frac{m}{\rho k_{0\rho}}\left(k_{0\rho}^2 + k_{0z}^2\right)E_{0k\phi}\mathrm{J}_m\right\}. \quad (80)$$

This form can be easily obtained from (74) and (75). Multiplying the terms in (74) and (75) by $-ik_{0z}$ and im/ρ, respectively, adding the resulting expressions, and multiplying it all by c^2/ω^2 yields (80). Using the same argument as before, it follows that, for the incoming wave, the expression on the left-hand side of (23) is a linear combination of the two expressions obtained from the left-hand side of (26).

It can be shown that the four expressions in (72) – (75) are linearly independent since the Bessel function and its derivative are linearly independent [21]. Thus, for the incoming plane wave, of the six terms contributing to the left-hand side of (23) – (26) only four are linearly independent.

From the form of the electric fields of the scattered waves and the waves inside the filament, the same discussion, as for the incoming wave, applies. The two wave modes, that appear in the fields for the scattered waves and for the waves inside the filament, can be treated independently of each other. Consequently, the combined electric fields that appear on either side of Eqs. (23) – (26) lead to just four independent boundary conditions.

---

[1] S. I. Krasheninnikov, *Phys. Lett. A* **283**, 368–370 (2001).

[2] S. J. Zweben, R. J. Maqueda, D. P. Stotler, A. Keesee, J. Boedo, C. E. Bush, S. M. Kaye, B. LeBlanc, J. L. Lowrance, V. J. Mastrocola, R. Maingi, N. Nishino, G. Renda, D. W. Swain, J. B. Wilgen, and the NSTX Team, *Nucl. Fusion* **44**, 134-153 (2004).

[3] J. R. Myra, D. A. D'Ippolito, D. P. Stotler, S. J. Zweben, B. P. LeBlanc, J. E. Menard, R. J. Maqueda, and J. Boedo, *Phys. Plasmas* **13**, 092509-1–092509-10 (2006).

[4] O. Grulke, J. L. Terry, B. LaBombard, S. J. Zweben, *Phys. Plasmas* **13**, 012306-1–012306-7 (2006).

[5] S. J. Zweben, R. J. Maqueda, J. L. Terry, T. Munsat, J. R. Myra, D. D'Ippolity, D. A. Russell, J. A. Krommes, B. LeBlanc, T. Stoltzfus-Dueck, D. P. Stotler, K. M. Williams, C. E. Bush, R. Maingi, O. Grulke, S. A. Sabbagh, and A. E. White, *Phys. Plasmas* **13**, 056114-1–056114-8 (2006).

[6] S. J. Zweben, J. A. Boedo, O. Grulke, C. Hidalgo, B. LaBombard, R. J. Maqueda, P. Scarin, and J. L. Terry, *Plasma Phys. Control. Fusion* **49**, S1–S23 (2007).

[7] D. A. Russell, J. R. Myra, and D. A. D'Ippolito, *Phys. Plasmas* **16**, 122304-1–056114-12

(2009).

[8] R. J. Maqueda, D. P. Stotler, and the NSTX Team, *Nucl. Fusion* **50**, 075002-1–075002-12 (2010).

[9] A. Yu. Pigarov, S. I. Krasheninnikov, and T. D. Rognlien, *Phys. Plasmas* **19**, 072516-1–072516-13 (2012).

[10] D. J. Griffiths, *Introduction to Electrodynamics* (Pearson, New Jersey, 1999, Third Edition) Chapter 7.

[11] K. Hizanidis, A. K. Ram, Y. Kominis, and C. Tsironis, *Phys. Plasmas* **17**, 022505 (2010).

[12] H. C. van de Hulst, *Light Scattering by Small Particles* (Dover, New York, 1957) Chapter 9.

[13] C. F. Bohren and D. R. Huffman, *Absorption and Scattering of Light by Small Particles* (Wiley-Interscience, New York, 1983) Chapter 4.

[14] A. K. Ram, K. Hizanidis, and Y. Kominis, *Phys. Plasmas* **20**, 056110-1–056110-10 (2013).

[15] A. K. Ram and K. Hizanidis, *Radiation Effects and Defects in Solids: Incorporating Plasma Science and Plasma Technology* **168**, 759–775 (2013).

[16] L. Tsang, J. Au Kong, and K-H. Ding, *Scattering of Electromagnetic Waves: Theories and Applications* (Wiley, New York, 2000) Chapter 1.

[17] J. D. Jackson, *Classical Electrodynamics* (Wiley, New Jersey, 1999, Third Edition) Chapter 7.

[18] T. H. Stix, *Waves in Plasmas* (Springer, New York, 1992) Chapters 1 and 2.

[19] J. A. Stratton, *Electromagnetic Theory* (McGraw Hill, New York, 1941) Chapters VI and VII.

[20] R. G. Barrera, G. A. Estévez, and J. Giraldo, *Euro. J. Physics* **6**, (1985) 287-294.

[21] M. Abramowitz and I. A. Stegun, *Handbook of Mathematical Functions* (Dover, New York, 1972) Chapters 8 and 10.

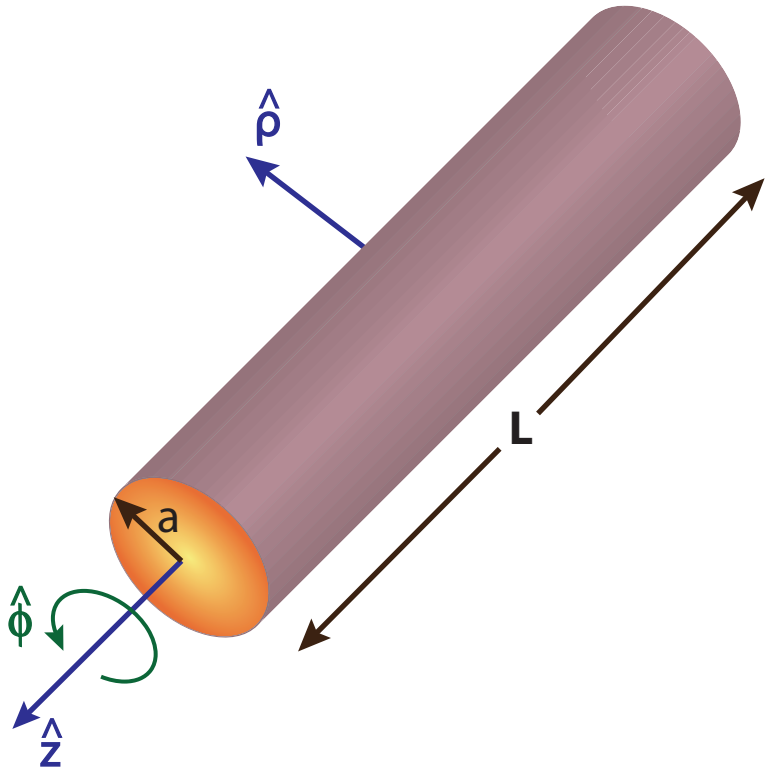

FIG. 1: The origin of the coordinate system is at the center of the cylindrical filament of radius a. The ambient magnetic field is along the axial direction $\hat{z}$, and $\hat{\rho}$ and $\hat{\phi}$ are the unit vectors along the radial and azimuthal directions, respectively. The effect of the ends of the filament are ignored by assuming that $L \to \infty$.

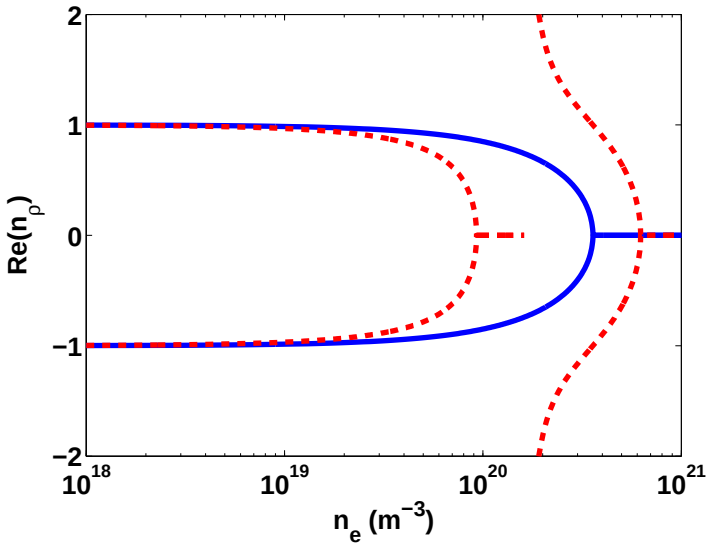

FIG. 2: (Color online) The real part of the radial, or perpendicular, wave number n_ρ as a function of the electron density n_e for electron cyclotron waves. The solid line corresponds to the ordinary wave while the dashed line is for the extraordinary wave. The wave frequency is 170 GHz, the parallel index of refraction $n_{0z} = 0$, and $B_0 = 4.5$ Tesla. The O wave is evanescent for $n_e \gtrsim 3.58 \times 10^{20}$ m^{-3}, while the X wave has two cutoffs and a resonance (the upper hybrid resonance).

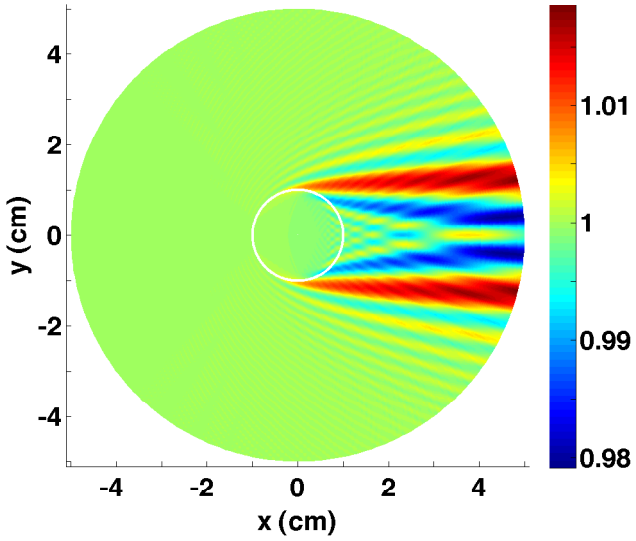

FIG. 3: (Color online) Contours of P_x in the $x - y$ plane for an incident O wave. The circular cross-section of the filament has a radius of 1 cm, and is indicated by the white circle. The relevant parameters are given in the text.

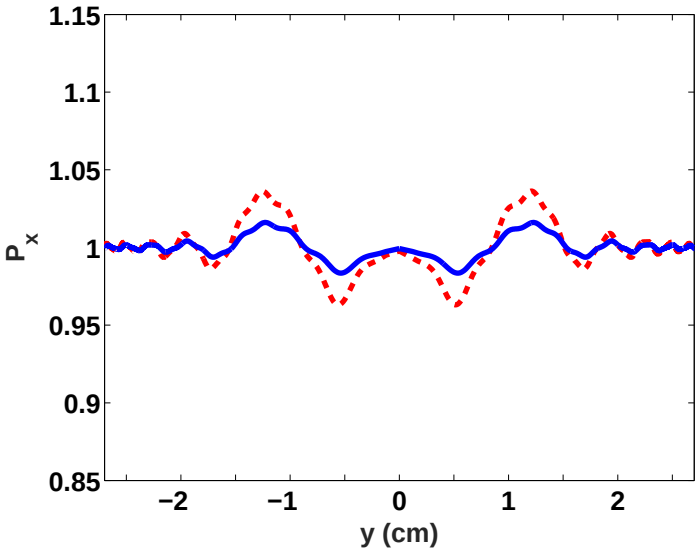

FIG. 4: (Color online) P_x versus y at $x = 2$ cm, corresponding to a location in the wake of the filament. The solid line corresponds to an incident O wave and the dashed line to an incident X wave. The shadowing effect occurs in regions where $P_x < 1$, while the focusing effect is for $P_x > 1$. For an incident O or X wave, $P_x^I = 1$. The wave and plasma parameters are the same as for Fig. 3.

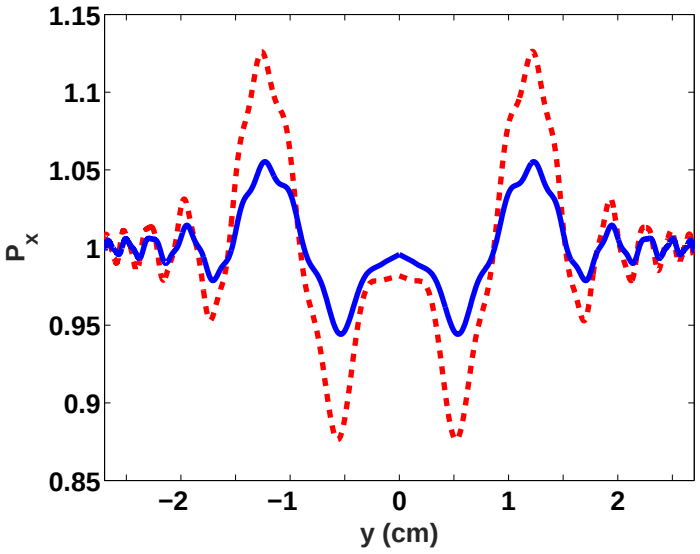

FIG. 5: (Color online) P_x versus y at $x = 2$ cm. The solid line corresponds to an incident O wave and the dashed line to an incident X wave. The plasma parameters are the same as for Figs. 3 and 4, except that the density inside the filament is $n_{ef} = 3.7 \times 10^{18}$ m^{-3}. The shadowing and focusing effects are more prominent when compared to Fig. 4 (drawn to the same scale). As before, for an incident O or X wave, $P_x^I = 1$.

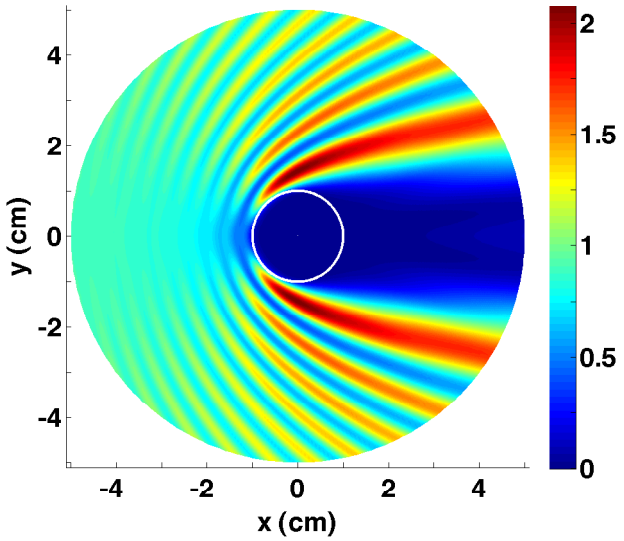

FIG. 6: (Color online) Contours of P_x in the $x-y$ plane for an incident O wave. In this case of a high density plasma, the O wave propagates in the background plasma but is cutoff inside the filament. The shadowing and focusing of the waves is evident. In contrast to Fig. 3, the diffraction pattern in the region $x < 0$ shows significant backscattering of the waves.

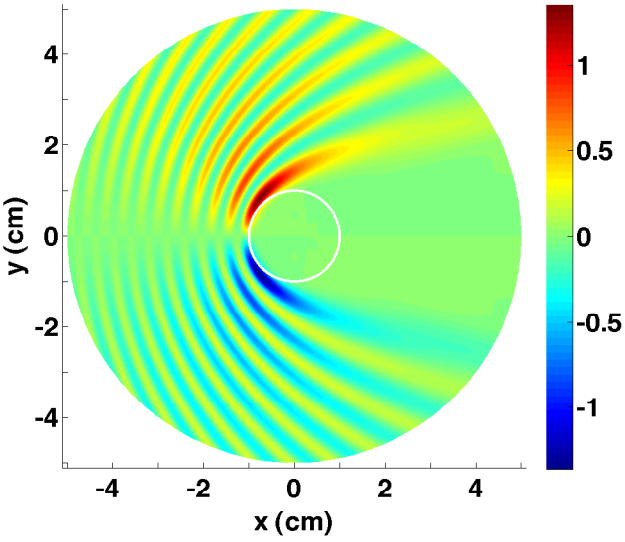

FIG. 7: (Color online) Contours of P_y in the $x-y$ plane for the same parameters as in Fig. 6. It shows side-scattering of the incident O wave in the wake of the filament as well as in the front of the filament facing the incoming wave. Side-scattering will lead to surface waves in a tokamak plasma.

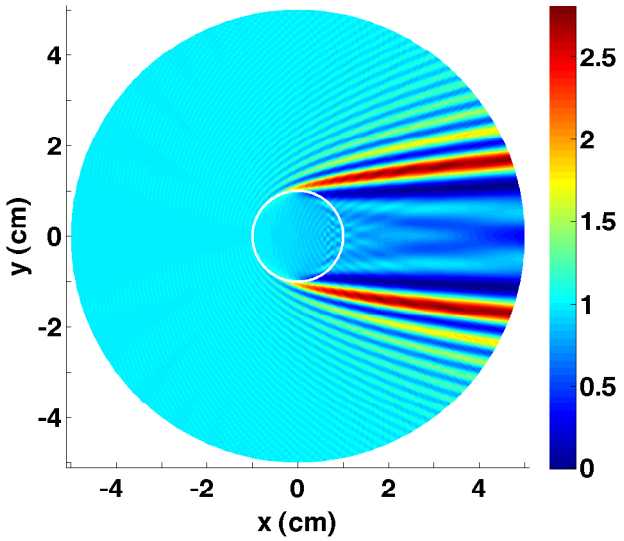

FIG. 8: (Color online) Contours of P_x in the $x-y$ plane when the X wave is incident on the filament. The X wave also propagates inside the filament. In contrast to the results in Fig. 6, there is essentially no backscattering. Also, the shadowing effect is reduced as the magnitude of P_x is not zero in the wake behind the filament.

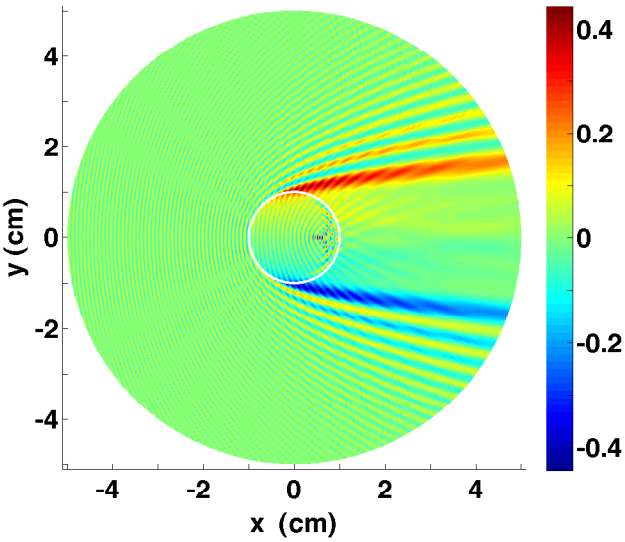

FIG. 9: (Color online) A contour plot of P_y in the $x-y$ plane for an incident X wave. Beside side-scattering in the forward direction, there are wave fields inside the filament. This is unlike the results in Fig. 6 and 7 where no fields are observed inside the filament.

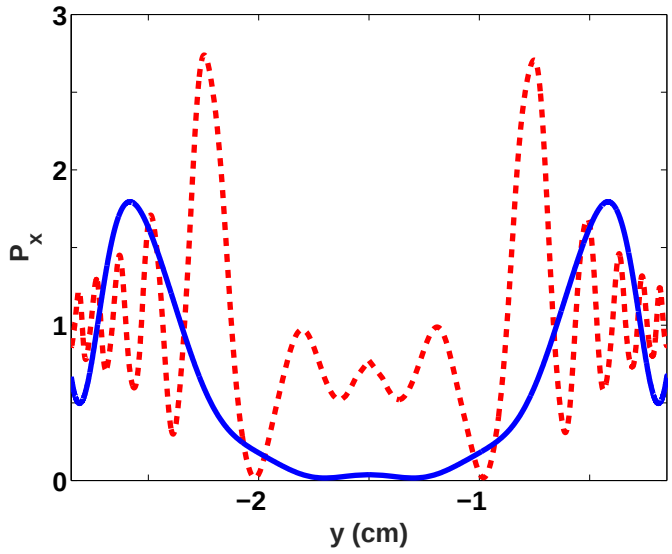

FIG. 10: (Color online) A comparison of P_x as a function of y at $x = 2$ cm (forward scattering) between an incident O wave (solid line) and X wave (dashed line). For the O wave, the shadowing effect is prominent, while for the X wave the Poynting flux into the core of the plasma is spatially structured. The parameters are the same as for Fig. 6.

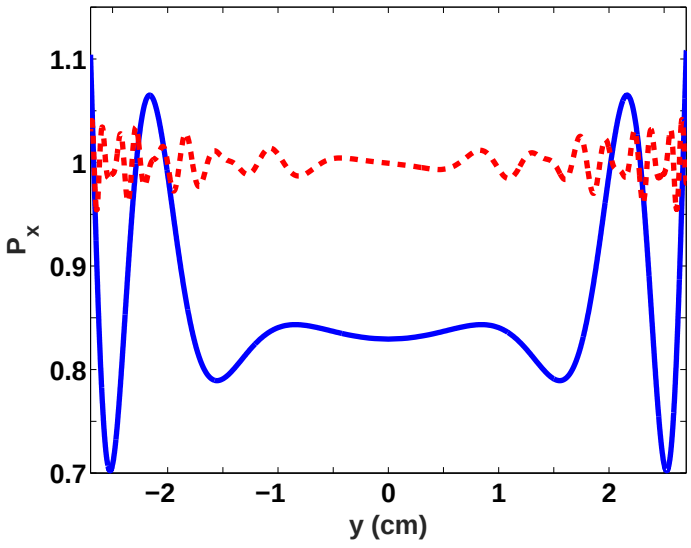

FIG. 11: (Color online) A comparison of P_x as a function of y at $x = -2$ cm (backward scattering) between an incident O wave (solid line) and X wave (dashed line). Since $P_x^I = 1$ for the incident wave, it is noticeable that there is effectively no backscattering of the X wave. The same is not true for the O wave.

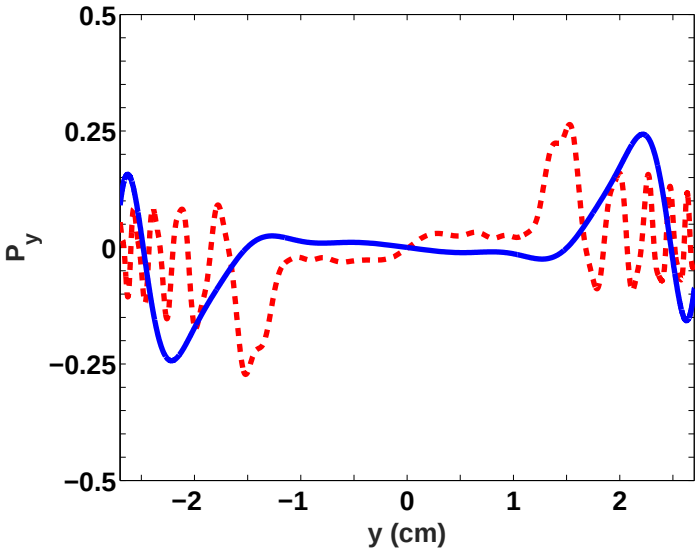

FIG. 12: (Color online) A comparison of P_y as a function of y at $x = 2$ cm between an incident O wave (solid line) and X wave (dashed line). Since $P_y^I = 0$ for either of the incident waves, the filament side-scatters some of the incoming wave power to surface waves that do not propagate into the core of the plasma.

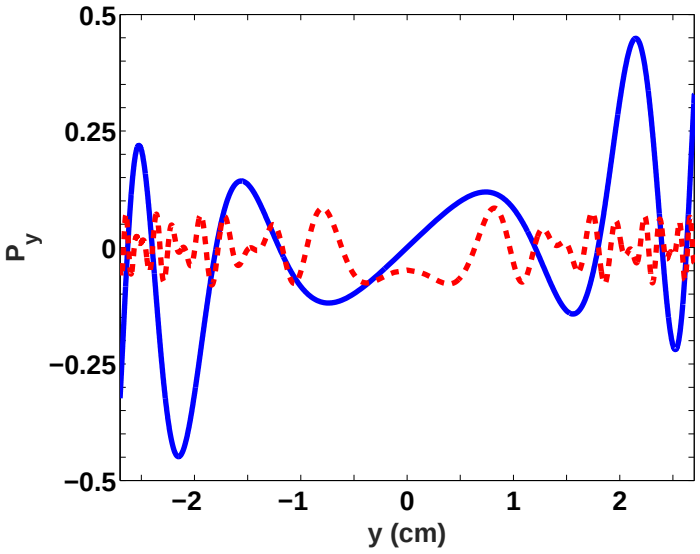

FIG. 13: (Color online) A comparison of P_y as a function of y at $x = -2$ cm between an incident O wave (solid line) and X wave (dashed line). The side-scattering is in front of the filament as opposed to the results in Fig. 12, in which the side-scattering is in the wake of the filament. There is essentially no side-scattering of the X wave; however, that is not the case for the O wave. The enhanced side-scattering of the O wave is correlated with the significant reflection of the wave (Fig. 6).

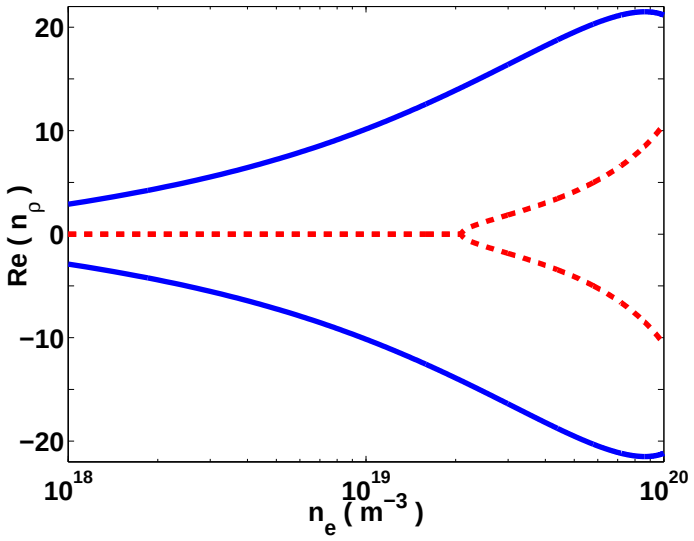

FIG. 14: (Color online) The real part of the radial, or perpendicular, wave number n_ρ as a function of the electron density n_e for lower hybrid waves. The solid line corresponds to the slow wave while the dashed line is for the fast wave. The fast wave is evanescent for densities $n_e \lesssim 2.09 \times 10^{20}$ m^{-3}. The wave frequency is 4.6 GHz, the parallel index of refraction is $n_{0z} = 2$, and $B_0 = 4.5$ Tesla.

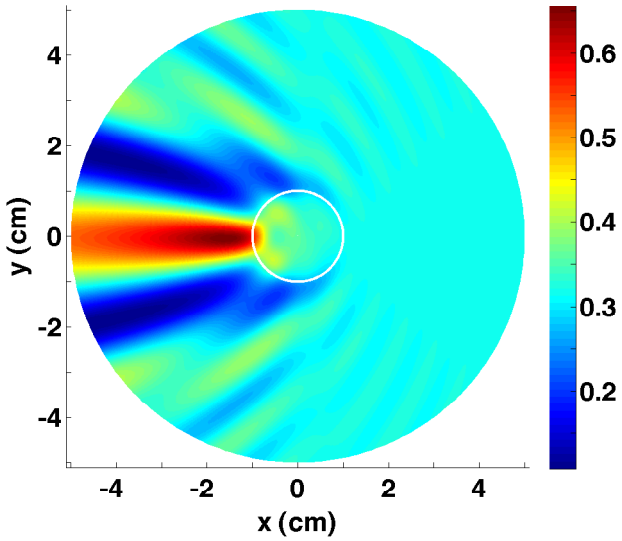

FIG. 15: (Color online) A contour plot of P_x in the $x-y$ plane for the low density case. Only the slow lower hybrid wave propagates in the background plasma and inside the filament. The wave is incident on the filament from the left-hand side as P_x is positive. The backscattering of the wave is obvious as the intensity of P_x is large for $x < 0$. The effects due to the interference between the incident and scattered waves are clearly discernible.

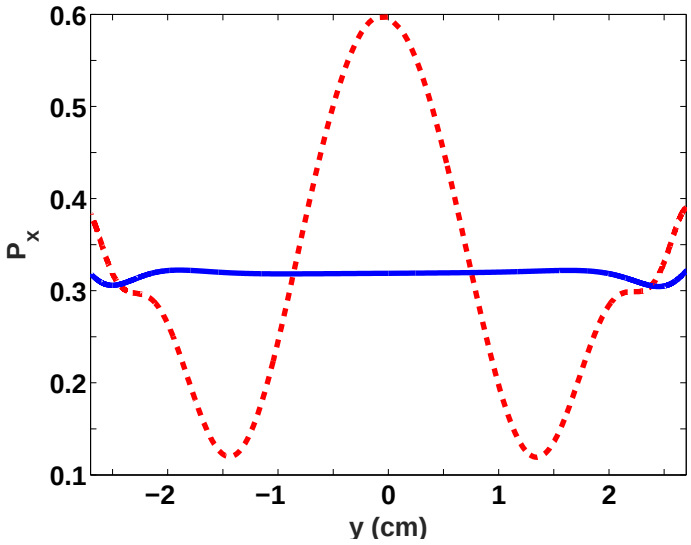

FIG. 16: (Color online) P_x versus y at $x = 2$ cm (solid line) and $x = -2$ cm (dashed line) as obtained from Fig. 15. For the incoming slow wave $P_x^I \approx 0.32$. The Poynting flux in the wake of the filament is not affected, while the interference between the incident and scattered waves is exhibited by the variations in P_x in the front of the filament (solid line). This is different from the scattering of the electron cyclotron waves as the slow hybrid wave is a backward wave. The interference patterns are formed by the phases of the incident and scattered waves.

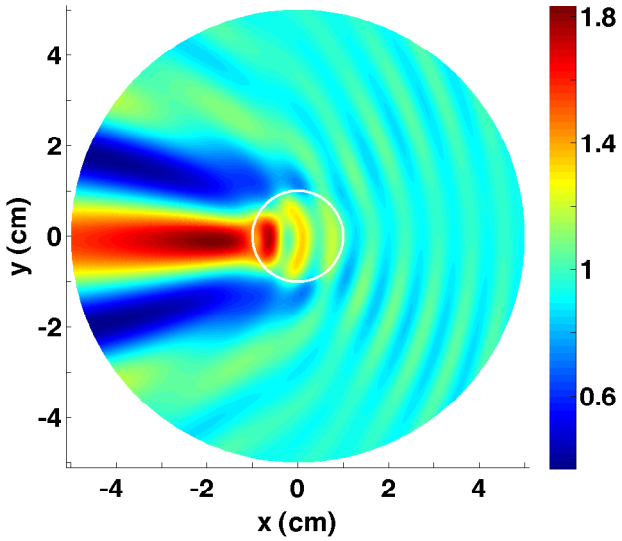

FIG. 17: (Color online) A contour plot of P_z in the $x-y$ plane for the same case as Fig. 15. For the incoming slow wave, $P_z^I \approx 0.95$. The high intensity inside the filament is illustrative of a transmission line behavior.

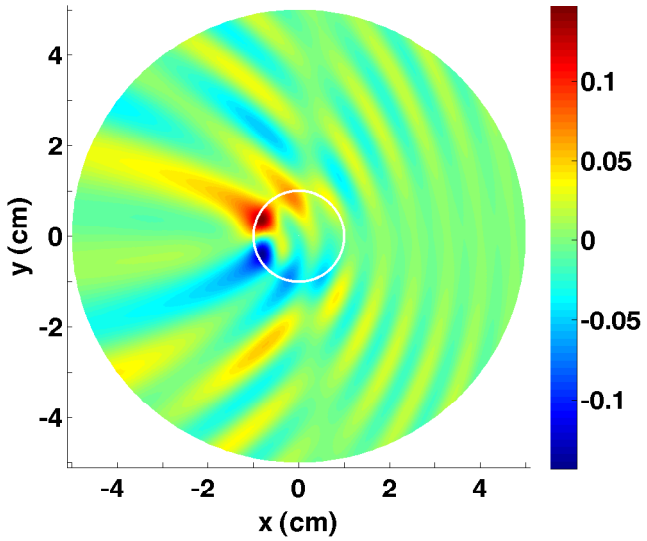

FIG. 18: (Color online) A contour plot of P_y in the $x-y$ plane showing side-scattering of the incident wave. The parameters are the same as Fig. 15 For the incoming slow wave, $P_y^I = 0$.

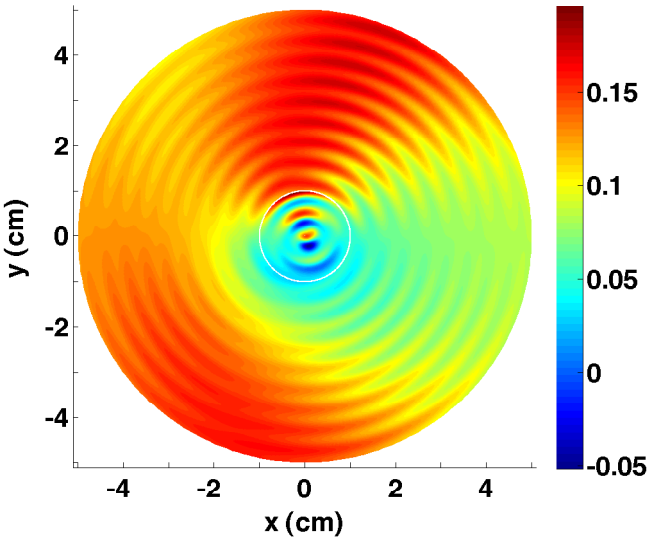

FIG. 19: (Color online) A contour plot of P_x in the $x-y$ plane for the case when the density inside the filament is less than the background density. The incident wave is the fast lower hybrid wave which is evanescent inside the filament. For the incident wave $P_x^I \approx 0.127$. The filament excites the slow lower hybrid wave in the background plasma. The radial distance between the peaks of two neighboring fringes outside the filament is approximately 0.45 cm, which, in turn, is approximately the wavelength of the slow wave in the background plasma.

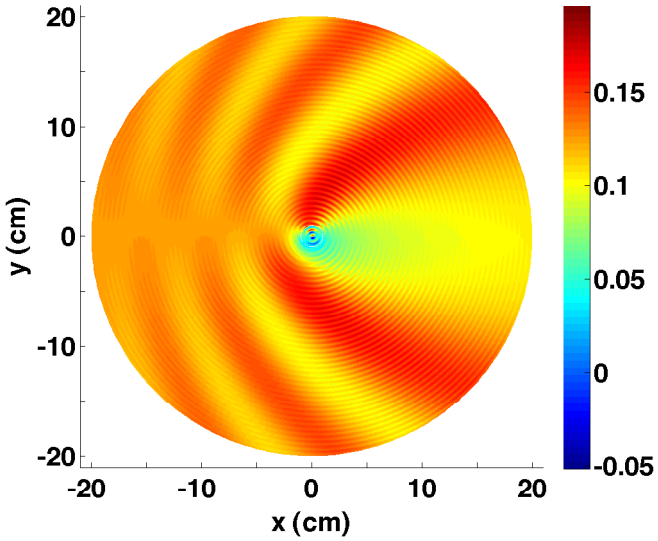

FIG. 20: (Color online) A contour plot of P_x in the $x-y$ plane. The parameters are exactly those used in Fig. 19 except that the scattering is viewed over a larger spatial domain $(x,y)\varepsilon[-20,20]$. The diffraction pattern occurs over a larger scale since the wavelength of the incident fast wave is approximately 11.3 cm. The importance of the filament, even though its radius is much smaller than the incident wavelength, is clearly depicted in this figure.